The wider context of the Lower Jurassic Toarcian Oceanic Anoxic Event in Yorkshire coastal outcrops, UK

Nicolas Thibault[a,*], Micha Ruhl[b], Clemens V. Ullmann[c], Christoph Korte[a], David B. Kemp[d], Darren R. Gröcke[e], Stephen P. Hesselbo[c]

[a] Department of Geosciences and Natural Resource Management, University of Copenhagen, Øster Voldgade 10, DK-1350 Copenhagen K, Denmark

[b] Department of Earth Sciences, University of Oxford, South Parks Road, Oxford OX1 3AN, UK

[c] University of Exeter, Camborne School of Mines & Environment and Sustainability Institute, Penryn Campus, Penryn, Cornwall TR10 9FE, UK

[d] School of Geosciences, University of Aberdeen, Aberdeen, AB24 3UE, UK

[e] Department of Earth Sciences, Durham University, South Road, Durham DH1 3LE, UK

* Corresponding author. Tel.: +45 35 32 33 50, E-mail address: nt@ign.ku.dk (N. Thibault).

Abstract

The Toarcian Oceanic Anoxic Event (T-OAE, ~183 Ma) was characterized by enhanced carbon burial, a prominent negative carbon-isotope excursion (CIE) in marine carbonate and organic matter, and numerous geochemical anomalies. A precursor excursion has also been documented at the Pliensbachian/Toarcian boundary, but its possible causes are less constrained. The T-OAE is intensively studied in the Cleveland Basin, Yorkshire, UK, whose sedimentary deposits have been litho-, bio- and chemostratigraphically characterized. Here, we present new elemental data produced by hand-held X-ray fluorescence analysis to test the expression of redox-sensitive trace metals and detrital elements across the upper Pliensbachian to mid-Toarcian of the Cleveland Basin. Detrital elemental concentrations (Al, Si, Ti, Zr) are used as proxies for siliciclastic grain content and thus, sea-level change, which match previous sequence stratigraphic interpretations from the Cleveland Basin. The timescale of the event is debated, though our new elemental proxies of relative sea level change show evidence for a cyclicity of 350 cm that may be indicative of ~405 kyr eccentricity cycles in Yorkshire. Trends in total organic carbon and redox-sensitive elements (S, Fe, Mo, As) confirm scenarios of widespread ocean deoxygenation across the T-OAE. The correlation of comparable trends in Mo across the T-OAE in Yorkshire and the Paris Basin suggests a similar oceanic drawdown of this element accompanying widespread anoxia in the two basins. Data from Yorkshire point to a transgressive trend at the time of the Mo drawdown, which contradicts the "basin restriction" model for the euxinic conditions that characterise the CIE interval.

Keywords: euxinia, Mo drawdown, cyclostratigraphy, sea level

1. Introduction

The Toarcian (~183 Ma ago, **Ogg et al., 2016**) was characterized by a severe environmental perturbation, associated with a major extinction of marine organisms (**Harries and Little, 1999**; **Caruthers et al., 2013**; **Danise et al., 2015**), enhanced carbon burial, and a pronounced negative carbon-isotope excursion (CIE) in marine carbonate and organic matter, and terrestrial organic matter (**Jenkyns, 1988**; **Hesselbo et al., 2000, 2007**; **McArthur et al., 2000; Bailey et al., 2003**; **Kemp et al., 2005**; **Hermoso et al., 2009, 2012**). Strong sedimentary TOC enrichment and (global) organic carbon burial, combined with the high abundance of redox sensitive trace metals and numerous geochemical anomalies (**Cohen et al., 2004**; **McArthur et al., 2008**; **Pearce et al., 2008**; **Gill et al., 2011**; **Kemp et al., 2011**; **Newton et al., 2011**) led to the recognition of a major Toarcian oceanic anoxic event (T-OAE). A pre-occurring companion of the early Toarcian CIE has also been documented at the Pliensbachian/Toarcian (P-To) boundary in marine carbonate, wood and/or marine organic matter in several European and North African basins, but its lithological expression and possible causes are at present poorly constrained and understood (**Hesselbo et al., 2007**; **Suan et al., 2010**; **Littler et al., 2010**; **Bodin et al., 2016**). Sections within the Cleveland Basin, UK, exposed along the northern coast of Yorkshire, have played a major role in the documentation of biotic and environmental changes prior to, during and after the T-OAE (**Howarth, 1962**; **Knox, 1984**; **Little and Benton, 1995**; **Harries and Little, 1999**; **Danise et al., 2013, 2015**). Here, we present a new high-resolution elemental dataset of hand-held X-ray fluorescence (XRF) analysis of the upper Pliensbachian to mid-Toarcian interval at Yorkshire coastal outcrops and review some of the major geochemical features of this interval. The expression of the P-To and T-OAE at Yorkshire coastal outcrops is discussed in its European context of sea-level and environmental change.

2. Geological setting

Sedimentary rocks of upper Pliensbachian to mid-Toarcian age are well exposed in the cliffs of the Yorkshire coast (Cleveland Basin, NE England) in the vicinity of Whitby (Fig. 1). The sampled successions have been the subject of numerous studies, and stand out due to their detailed lithostratigraphic descriptions, geochemical characterization, and precise (ammonite) biozonation (**Howarth, 1955, 1973, 2002**; **Howarth *in* Cope et al., 1980**; **Hesselbo and Jenkyns, 1995**). The sedimentology and biostratigraphy are very well known and described in **Howarth (1955, 2002)**, **van Buchem and Knox (1998)**, **Hesselbo and Jenkyns (1995)** and **Hesselbo et al. (2000)**. The stratigraphic and geographic framework applied in this study follows that of **Hesselbo and Jenkyns (1995)** and **Howarth (2002)**. Sediments analysed here originate from the late Pliensbachian Cleveland Ironstone Formation and Toarcian Whitby Mudstone Formation. The Cleveland Ironstone Formation is characterised by grey shales, with numerous sideritic concretionary horizons. The Pliensbachian-Toarcian transition is marked by four decimeter-thick, pyrite-rich shales named "sulfur bands". The early to mid-Toarcian of the Whitby Mudstone Formation is characterised by monotonous dark grey mudstones with carbonate and rare sideritic concretions. Two intervals of these dark grey shales are laminated from 10 to 34 m (unit 2 to unit 4a in this study, Fig. 2), and from 42.5 to 48.5 m which corresponds to the base of the Alum Shale Member (Fig. 2). Correlation between sections of Pliensbachian to Toarcian strata is possible at the decimeter scale over kilometres of the Yorkshire coast because of the detailed ammonite biostratigraphy and of the presence of the sideritic concretions (abundant in the late Pliensbachian, rarer in the early Toarcian), of numerous marker beds of carbonate, and of numerous layers with carbonate concretions of characteristic shapes and size (e.g. cannonballs,

whale stones, mill stones, Howarth, 1955, 2002). Sections at Staithes (upper Pliensbachian), Hawsker Bottoms (upper Pliensbachian to lower Toarcian) and Saltwick Nab (lower to mid-Toarcian), have been selected for this study (Toarcian, Fig. 2). Bed numbering is identical to that given in **Hesselbo and Jenkyns (1995)**.
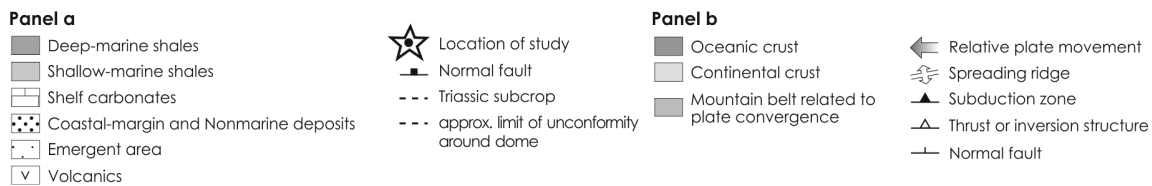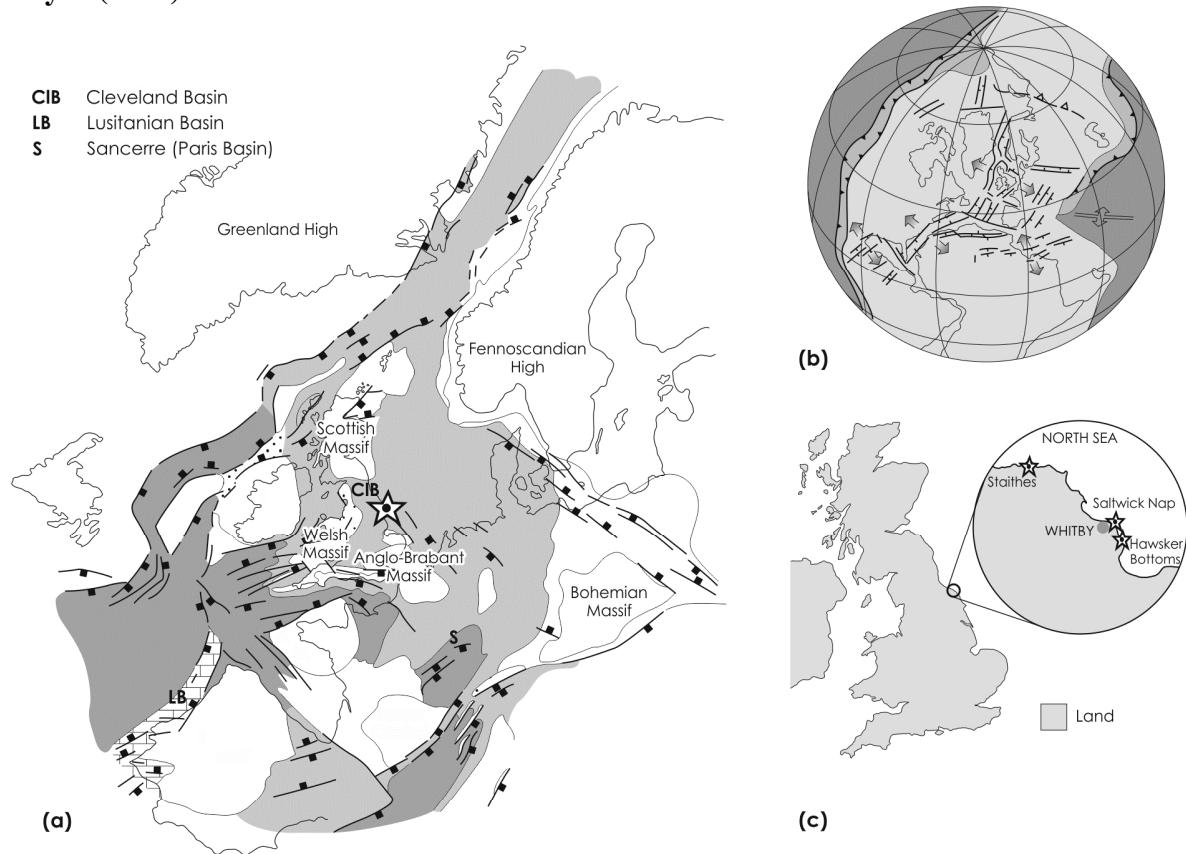

Figure 1. Early Jurassic palaeogeography of the studied area (a and b) modified after **Coward et al. (2003)** and **Korte and Hesselbo (2011)**, with localities (stars) sampled (c). The star (a) marks the Yorkshire coastal outcrops in the Cleveland Basin (UK) situated in the Early Jurassic at 35–40°N.

3. Methods

3.1. Hand-held XRF analyses

A total of 336 samples have been analysed from the top of the Pliensbachian Subnodosus ammonite subzone of the Margaritatus ammonite Zone, to the Toarcian Commune Subzone of the Bifrons ammonite Zone (Fig. 2, Appendix A). Average sample resolution varied, from ~70 cm in the Gibbosus Subzone to Apyrenum Subzone, to ~25 cm in the Hawskerense Subzone to base Tenuicostatum Subzone, ~8.6 cm in the Tenuicostatum Subzone to Exaratum Subzone, ~23 cm in the Falciferum Subzone and ~51 cm in the Commune Subzone of the Bifrons Zone. Major- and minor elemental
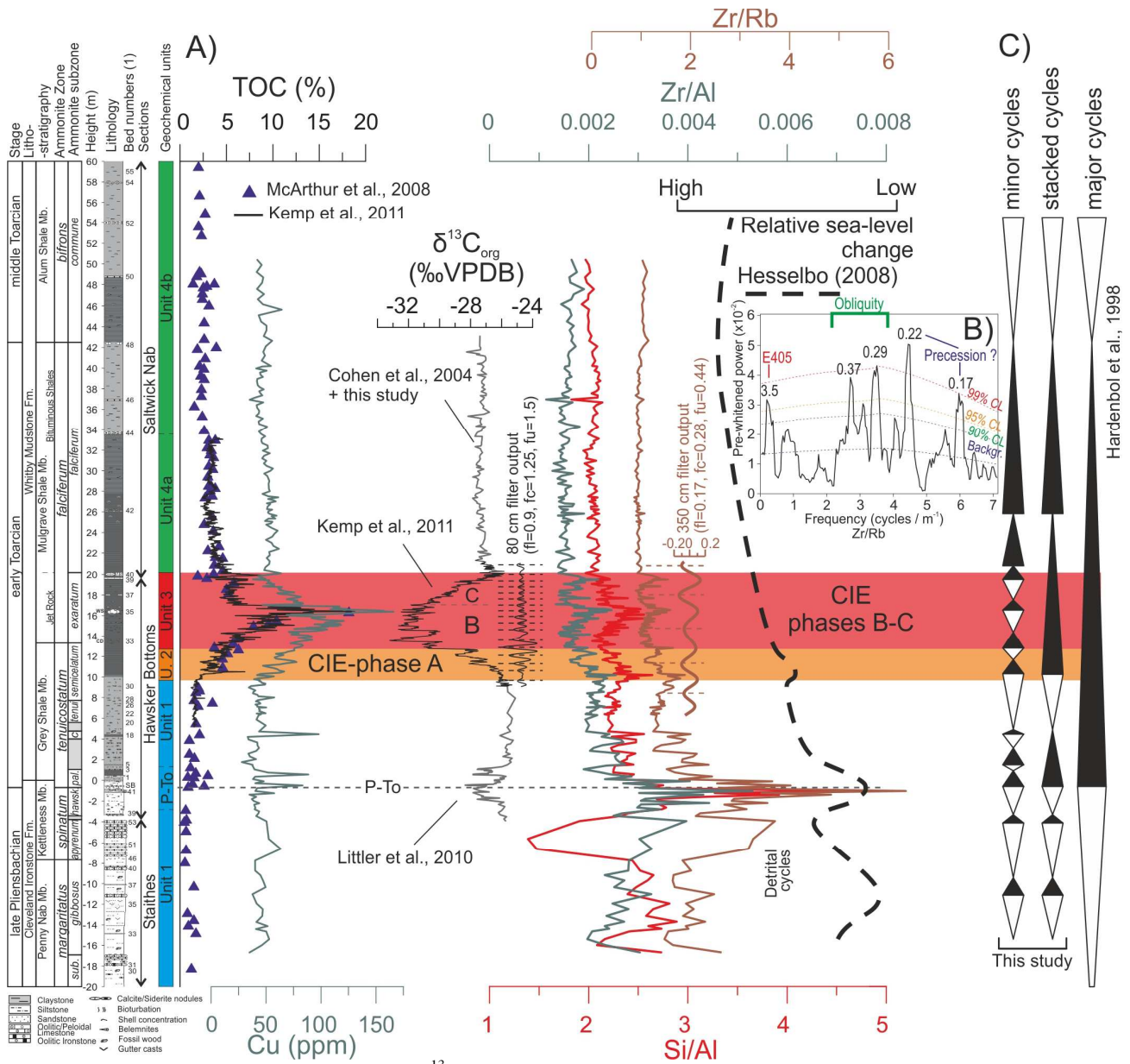
Figure 2. A) %TOC and Cu concentration, $\delta^{13}C_{org}$ and trends in the ratio of siliciclastic elements (Zr/Al, Si/Al, Zr/Rb) compared to the relative sea-level curve of **Hesselbo (2008)**. For the Toarcian carbon isotope excursion, we distinguish an interval corresponding to the onset of a progressive decrease in carbon isotopes (phase A of the CIE or Unit 2) and the remaining of the CIE (phases B-C) corresponds to geochemical Unit 3, whose base is defined by the first sharp, major drop in $\delta^{13}C_{org}$. A 80 cm filter output of $\delta^{13}C_{org}$ data (Based on **Kemp et al., 2005, 2011**) is also presented along with an interpretation of the different cycles through the CIE interval (fl = lower cut-off, fc=central frequency, fu = upper cut-off. B) 2π MTM periodogram of the Zr/Rb ratio showing a significant periodicity of 360 cm. Extraction of this periodicity is shown in the filter output next to the Zr/Rb curve. C) Minor transgressive-regressive cycles are deduced from the observation of common detrital cycles in Zr/Al, Si/Al and Zr/Rb and a stacking of these cycles is proposed. Major cycles correspond to previously recognized 2nd order sequences based on the major sequence boundary at the Pliensbachian/Toarcian boundary (**Hesselbo, 2008**; MRS Pl8 of **Hermoso et al., 2013**) and on the major MFS at the transition from the Serpentinum to the Bifrons zones (**Gély and Lorenz, 2006**; **Hesselbo, 2008**; **Hermoso et al., 2013**). (1) Bed numbers following **Howarth (2002)**.

5

concentrations were determined from powdered rock samples using an Olympus DP-6000 handheld XRF analyser (HH-XRF), with a Rh tube, and with 40 and 10 kV beam currents, respectively. Calibration of this device is described in **Dahl et al. (2013), Lenniger et al. (2014)** and **Ahm et al. (2017)** for most elements used here, except for sulphur which has been further calibrated by a correction factor of 1.61 by comparison to the previous high-resolution C-N-S analyser results of **Kemp et al. (2011)**. Iron has been further recalibrated by a correction factor of 0.85 by comparison to ICPMS-data from **McArthur et al. (2008)**. These two correction factors have been calculated by re-interpolating the data of **McArthur et al. (2008)** and **Kemp et al. (2011)** to the stratigraphic height of our own samples and calculating a line of regression with zero intercept between the two sets of measurements (Appendix B). Arsenic (As) was not considered in the elemental dataset of **Ahm et al. (2017)** and constitutes one of the standard elemental targets in generations of HH-XRF devices for assessing soil pollution (**Potts and West, 2008**). The detection limit provided for As by the Olympus DP-6000 HH-XRF provider is estimated at 9 ppm in the absence of lead (Pb). Only twelve samples of our dataset yield values in As slightly below this detection limit with a minimum measured value of 7.4 ppm (Appendix A). Arsenic is considered by the provider as a straightforward, well-calibrated element, and precisions on As results may only be affected when the concentration in Pb is high. Less than 5% of our samples have Pb contents higher than 40 ppm and the precision on As with such concentrations in Pb is 15 ppm and 8 additional samples yield As values which are below the detection limit when Pb content is higher than 40 ppm (Appendix B). Relevant trends highlighted for As and discussed further in this manuscript are based on values that are higher than these detection limits.

For sample preparation, sediments were dried, in vacuum, in a freeze-drier for 48 h and then powdered. Powders were subsequently stored in plastic containers, which were covered with a single layer of kitchen wrap. In order to ensure reproducible results, the brand of the 'kitchen wrap' remains systematically the same at Copenhagen (Køkkenchefen Husholdningsfilm produced for Dansk Supermarked A/S). A total thickness of 1 cm of powder was analysed for all samples which is far beyond the recommended minimum thickness of 0.4 cm (**Dahl et al., 2013**; **Mejía-Piña et al., 2016**). A total exposure time of 180 s was used (90 s on each beam) as recommended by the manufacturer and in **Mejía-Piña et al. (2016)**. Comparison of XRF versus ICP-MS measurements shows that the average relative external uncertainty across all recorded elements is within 13 %, and the instrumental error is generally less than 10% (**Ahm et al., 2017**).

3.2. Organic carbon isotopes

A total of 90 samples have been analysed for carbon isotopes in bulk organic matter ($\delta^{13}C_{org}$), in the interval between 21.8 m and 42 m (Fig. 2) at Oxford University, following the method described in **Gröcke (2002)**. These data were combined with the data of **Cohen et al. (2004)**, **Kemp et al. (2005)** and **Littler et al. (2010)** to produce an extended high-resolution composite dataset of bulk organic carbon isotope evolution across the upper Pliensbachian and lower Toarcian strata in the Cleveland Basin (Appendix C).

3.3. Multivariate statistics and data standardisation

To compare all geochemical proxies in the same data matrix, compiled total organic carbon (TOC), %CaCO$_3$ and $\delta^{13}C_{org}$ data from the literature (**McArthur et al., 2008**; **Kemp et al., 2011**), were re-interpolated to reflect the same data-resolution as major and minor elemental XRF concentration data. This data-matrix was subsequently used to perform principal component and cluster analysis in the PAST software (**Hammer et al., 2001**). Most samples from the upper Pliensbachian at Staithes present

very high anomalies in trace metal concentrations, and these samples were therefore not considered for multivariate statistics. The elements U, Ni, Y, Hg, Pb, and Th were measured, but had concentrations near or below detection limit throughout most of the studied succession. These elements are therefore not considered further here. For a few Toarcian samples, the concentration of some trace elements considered in this study were below detection limit and these samples were therefore removed from the data matrix. Out of the 336 samples analysed in this study, the final matrix used for statistical analyses is composed of data from a total of 292 samples. The matrix was centred and reduced using the mean and standard deviation of each variable prior to multivariate statistics (Appendix D). For a number of elements (e.g. Mo, As), enrichment factors have been calculated as $EF_{element\ X} = (X/Al_{sample})/(X/Al_{average\ shale})$. Average shale values for these elements are taken from **Turekian and Wedepohl (1961)** and **Wedepohl (1971)**. The degree of pyritization of total Fe (DOP-T) has been calculated as Total S/Total Fe, and this in contrast to **McArthur et al. (2008)** who accounted for a 5% fraction of total sulphur bound to organic matter. In the present study the potential organic-bound sulphur fraction is not subtracted representing the maximum concentration of the potential sedimentary pyrite and, moreover, allowing for a direct comparison to prior DOP-T datasets of the literature (e.g., **Algeo and Maynard, 2004**; **Berner et al., 2013**). Non-reactive Fe (detrital and in siderite) was estimated by assuming that all reactive Fe was pyritized and calculated as the difference between total Fe (measured by XRF) and Fe in pyrite (Fe_{pyrite} = S/1.143 according to its concentration of 46.7% vs. 53.3% S in stoichiometric pyrite).

3.4. Sequence stratigraphy and cyclostratigraphy

The sedimentary ratio between some detrital elements (e.g. Si/Al, Zr/Al, Zr/Rb) is sensitive to changes in the type of siliciclastic grains and minerals and thus, may potentially reflect sediment transport distance and transport energy (**Govin et al., 2012**), In particular, the Zr/Rb ratio is related to grain-size variation in the sediments, which depends on the distance from the clastic source and transport energy; Zr occurs structurally in zircon, a heavy mineral, generally transported over short distances, whereas Rb is a light element, present in K-feldspar, mica and clay minerals, transported over long distances (**Liu et al., 2004**; **Chen et al., 2006**; **Aquit et al., 2017**). Trends in these sedimentary ratios can reflect proximal to distal trends expressed as cyclic changes, which may be interpreted in terms of transgressive-regressive facies sequences. Maximum Flooding Surfaces and Maximum Regressive Surfaces (MFS, MRS, respectively) have been interpreted in these proxies as local minima and maxima of the curves. The periodicity of the cyclic pattern of Zr/Rb across the T-OAE was studied in the interval from 6.3 to 19.5 m using spectral analysis performed via a LOWSPEC spectrum on the linear-detrended and padded time-series in the Astrochron package (Meyers, 2014). LOWSPEC is a 'robust' method for spectral background estimation, designed for the identification of potential astronomical signals that are embedded in red noise (Meyers, 2012). Initial pre-whitening with AR1 filter offers the opportunity with this method to focus particularly on the high frequencies. Prior to this analysis, the Zr/Rb data were evenly interpolated at 7 cm. Observed specific frequencies highlighted by spectral analysis, were extracted using Taner filters (Taner, 2000).

4. Results

4.1. Multivariate statistics

4.1.1. Subdivision into stratigraphic intervals

The comparison of our HH-XRF dataset versus Kemp et al. (2005, 2011) and McArthur et al. (2008) show an excellent match in the trends and range of values reproduced for various elements (Fig. 1 for TOC, Fig. 6 for Mo, Fig. 7 for S and Fe). This comparison rules out potential lateral changes in facies and associated lateral changes in element concentrations between the distant sections sampled here as an explanation for observed stratigraphic variations for the following reasons: (1) most of the late Pliensbachian was sampled by us at Staithes whereas the late Pliensbachian of **McArthur et al. (2008)** was sampled at Hawsker Bottoms, (2) the P-To and T-OAE intervals were sampled by us at Hawsker Bottoms (top at 20 m) whereas they were sampled at Port Mulgrave (close to Staithes) by **McArthur et al. (2008)**, (3) a drastic drop in the concentration of total Fe and S is similarly recorded in our dataset and in that of **McArthur et al. (2008)** exactly at the transition between the Exaratum and Falciferum subzones (20 m) despite the fact that, contrary to us, McArthur et al. sampled this transition at the same location (Port Mulgrave) up to 24 m. (4) Despite the fact that McArthur et al. sampled another location above 24 m (Saltwick Nab), there is no significant change in his element dataset below (Hawsker Bottoms samples) and above that level (Saltwick Nab samples). Changes observed in geochemical proxies thus appear to be independent of the locations chosen along the Yorkshire coast and various locations appear to show reproducible trends.

A cluster ordination of the 292 samples was performed in order to define distinct geochemical units along the studied upper Pliensbachian to mid-Toarcian succession (Fig. 3). The results suggest four distinct units:
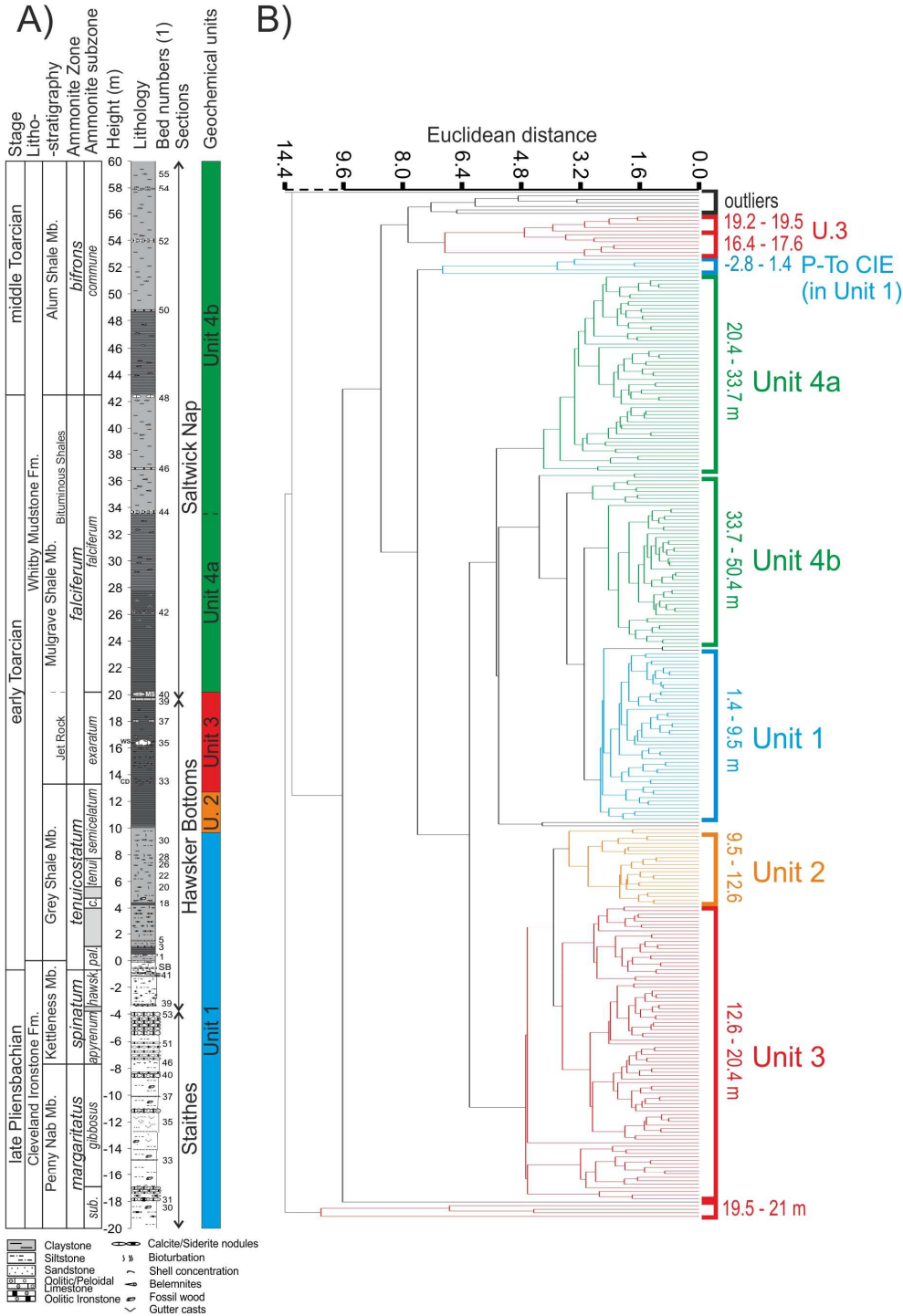
Unit 1 corresponds to strata of the Margaritatus to Tenuicostatum zones, directly preceding the base of an interval of laminated black shale within the Semicelatum Subzone (Fig. 3). Within Unit 1, strata of the P-To CIE interval are characterised by a significant increase in Si/Al, Zr/Al and Zr/Rb ratios and more negative values in $\delta^{13}C_{org}$ (Fig. 2), clearly separating them from the remainder of Unit 1 and constituting a small, but distinctive, sub-unit (Fig. 3).

Unit 2 roughly corresponds to the upper half of the Semicelatum Subzone and is characterised at the base of the laminated black shales with a progressive increase in TOC and a stepwise, progressive, decrease in $\delta^{13}C_{org}$ (Fig. 2). Unit 2 thus corresponds to the initiation of the CIE of the T-OAE and is further referred to as 'CIE Phase A' interval.

Unit 3 essentially spans the Exaratum Subzone and corresponds to the main negative CIE interval (Fig. 3). Its base coincides with the first major decrease in $\delta^{13}C_{org}$ (at ~12.5 m) and its top with a local maximum in $\delta^{13}C_{org}$ corresponding to the end of the full recovery or rising limb of the CIE (Fig. 2). Unit 3 is also characterised by the highest values in TOC (Fig. 2) as well as numerous geochemical anomalies which are described in detail below.

Unit 4 spans the Falciferum to *Commune* subzones and corresponds to the interval overlying the CIE where $\delta^{13}C_{org}$ values remain stable around -27.5‰ (Fig. 2). Sample cluster ordination possibly reflects a distinct Sub-unit 4a, corresponding to the laminated black shales of the Falciferum Subzone, and of a distinct Sub-unit 4b spanning the upper half of the Falciferum Subzone to the top of the studied interval in the Bifrons Zone (Fig. 3).

Figure 3. A) Lithologic log and stratigraphy of the section with the distinct geochemical units. B) cluster ordination of the samples performed on the centred-reduced matrix described in section 3.3. (1) Bed numbers following **Howarth (2002)**.

4.1.2. Elemental patterns of cluster ordination and principal component analysis
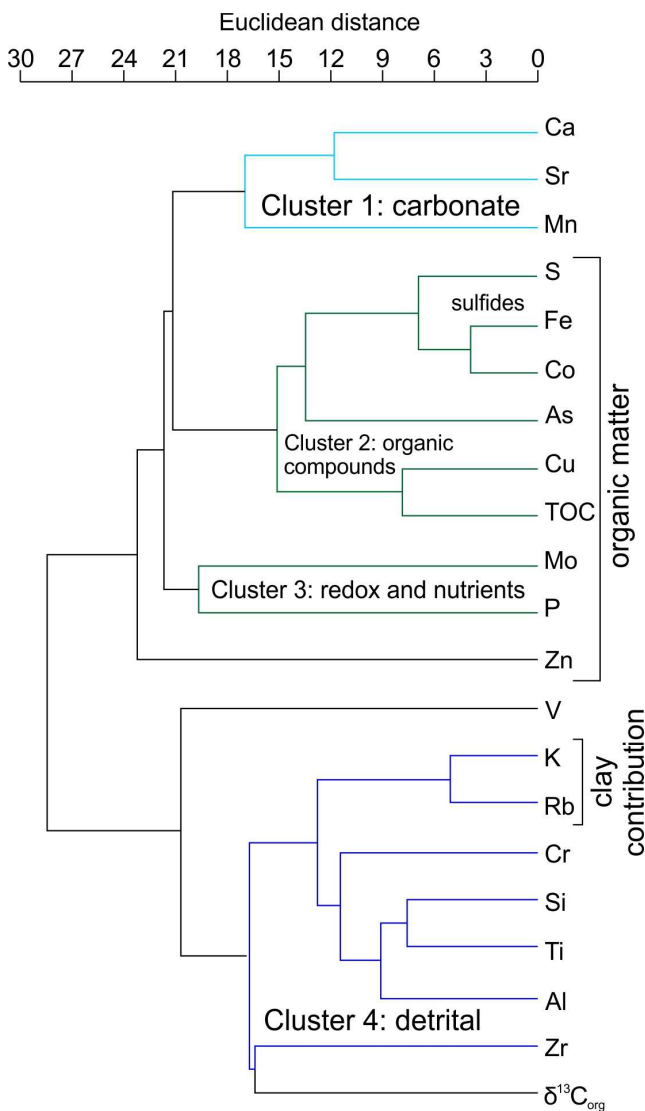
The major (Al, K, S, Ca, Fe, Mg, Si), minor and trace (P, Ti, V, Cr, Mn, Co, Ni, Cu, Zn, As, Rb, Th, Sr, Zr, Mo) elemental compositions of the studied bulk-rock samples reflect the varying proportions of lithogenic, biogenic and hydrogenic components in the sediments. Results of a cluster ordination of the different variables point to the different grouping of 'carbonate' elements (e.g. Ca, Sr, Mn) and sulphide-associated elements (e.g. S, Fe, Co) along with elements bound to organic compounds (As, Cu) and TOC (Fig. 4). Nutrient-related elemental concentrations (e.g. P) and redox-state related elemental concentrations (e.g. Mo) are grouped in a sister cluster (Fig. 4). All detrital elements (K, Rb, Cr, Si, Ti, Al and Zr) are grouped along with $\delta^{13}C_{org}$. A sub-cluster of elements maybe distinguished (e.g. K, Rb), which are specifically associated with the clay contribution to detritism. Three distinct components are considered here from Principal Component Analysis (PCA) which together explain nearly three quarters of the observed variance of the dataset: PC1 contributes ~48.5% of the total variance and has high positive loadings of Al, Si, K, Ti, Cr, Rb and Zr *vs*. high negative loadings of S, Ca, Fe, Co, Cu and TOC (Table 1). PC2 contributes ~13.5% of the total variance and has high positive loadings of S, Co, Cu and TOC *vs*. high negative loadings of P, Ca, Mn, Sr and $\delta^{13}C_{org}$. PC3 contributes ~11.5% of the total variance and shows high positive loadings of P, K, As, Rb, Mo *vs*. high negative loadings of Mn and Zr, but no significant loadings of either Ca or TOC (Table 1).

Trends in PC1 show a clear correlation to Al and an anti-correlation to the sum of %CaCO$_3$ and %TOC that likely reflects a closed-sum effect (Fig. 5, Table 1). Component loadings of PC2 show an opposition of carbonate constituents versus organic matter constituents (Fig. 5, Table 1). Positive trends of this component mostly highlight the progressive increase and decrease of organic matter in the sediments of the CIE interval (Units 2 and 3). Negative trends highlight intervals with anomalously high carbonate content that are associated with carbonate nodules, and therefore carbonate diagenesis. Component loadings and trends observed in PC3 reflect the strong influence of principally Mo and As (Fig. 6, Table 1). The positive contribution of K and Rb versus the negative contribution of Mn to PC3 principally reflects the expression of the three anomalous peaks in carbonate at 1 m, 16.4 m and 19.7 m associated with carbonate/siderite nodules (Table 1). The negative loading of Zr on PC3 remains enigmatic. Opposing signals for Zr and Mo (or As), the rather low contribution of aluminosilicates to this factor, and the complete independency of this factor from carbonate elements and organic matter, however, suggest that Mo and As concentrations in the sediments cannot only be explained by the variable admixture of lithogenous (detrital) and biogenic (CaCO$_3$, C$_{org}$) components. The study of Mo and As behaviours with respect to the distinct facies and geochemical units thus appears important in our dataset.

4.2. S/TOC ratio

Samples of the black shales from Unit 2 and Unit 3 plot along a regression line with a slope of 0.23%S per %TOC and an intercept of 3.5 %S on the sulphur axis (Fig. 7B). Although the intercept is different, the steepness of the slope compares well with that (0.18) of the Posidonia shale from the Weilstetten core (southwest Germany) (**Berner et al., 2013**). Such regression parameters have been interpreted as indicative of sediments deposited under anoxic conditions (**Berner et al., 2013**). In contrast, the data of Units 1 and 4 plot along regression lines that are much steeper and almost equal, close to 1.2% S per %TOC. The difference in the intercepts of these two regression lines, however, is substantial, as sediments of Unit 1 show a regression line that passes through the origin, possibly suggesting normal marine bottom-water conditions (**Berner et al., 2013**). The high steepness of the slope compared to

modern normal marine sediments (0.36, Fig. 7B) may suggest an excess of sulphur relative to the amount of organic carbon, which could be related to diagenetic sulphurization affecting sediments situated below the black shales by non-reacted downward diffusion of H_2S/HS^- (**Berner et al. 2013**). The negative intercept of -1.1% S of the regression slope of Unit 4 may indicate an excess in TOC relative to sulphur in sediments of Unit 4. This finding is intriguing because sediments of Unit 4a correspond to laminated black shale facies with a sulphur content >2% (Fig. 8) which, for a number of reasons discussed in the following sections, have also been interpreted as deposited under anoxic conditions, albeit not as restricted conditions as sediments of Units 2 and 3 (**McArthur et al., 2008**).

Figure 4. Results of the Cluster ordination of the variables performed on the centred-reduced matrix described in section 3.3.

	PC 1 (48.5%)	PC 2 (13.5%)	PC 3 (11.5%)
Al	**0.27**	0.16	0.18
Si	**0.27**	0.18	-0.06
P	-0.06	**-0.24**	**0.21**
S	**-0.27**	0.24	0.06
K	**0.24**	0.20	**0.25**
Ca	**-0.22**	**-0.39**	0.01
Ti	**0.30**	0.08	-0.02
V	0.12	-0.18	0.10
Cr	**0.28**	-0.04	-0.03
Mn	-0.19	**-0.22**	**-0.32**
Fe	**-0.27**	0.20	0.13
Co	**-0.25**	0.24	0.13
Cu	**-0.22**	**0.31**	-0.11
Zn	-0.03	-0.03	0.06
As	-0.19	0.07	**0.41**
Rb	**0.23**	0.16	**0.30**
Sr	-0.11	**-0.44**	0.20
Zr	**0.21**	0.02	**-0.27**
Mo	-0.07	-0.07	**0.55**
TOC	**-0.25**	0.19	-0.10
$\delta^{13}C_{org}$	**0.22**	**-0.30**	0.08

Table 1: Loading coefficients for PC1 to PC3 of the different variables of the variance-covariance matrix resulting from the principal component analysis (PCA). Percentage of the total variance is indicated for each component. High positive and negative loadings are highlighted in bold.
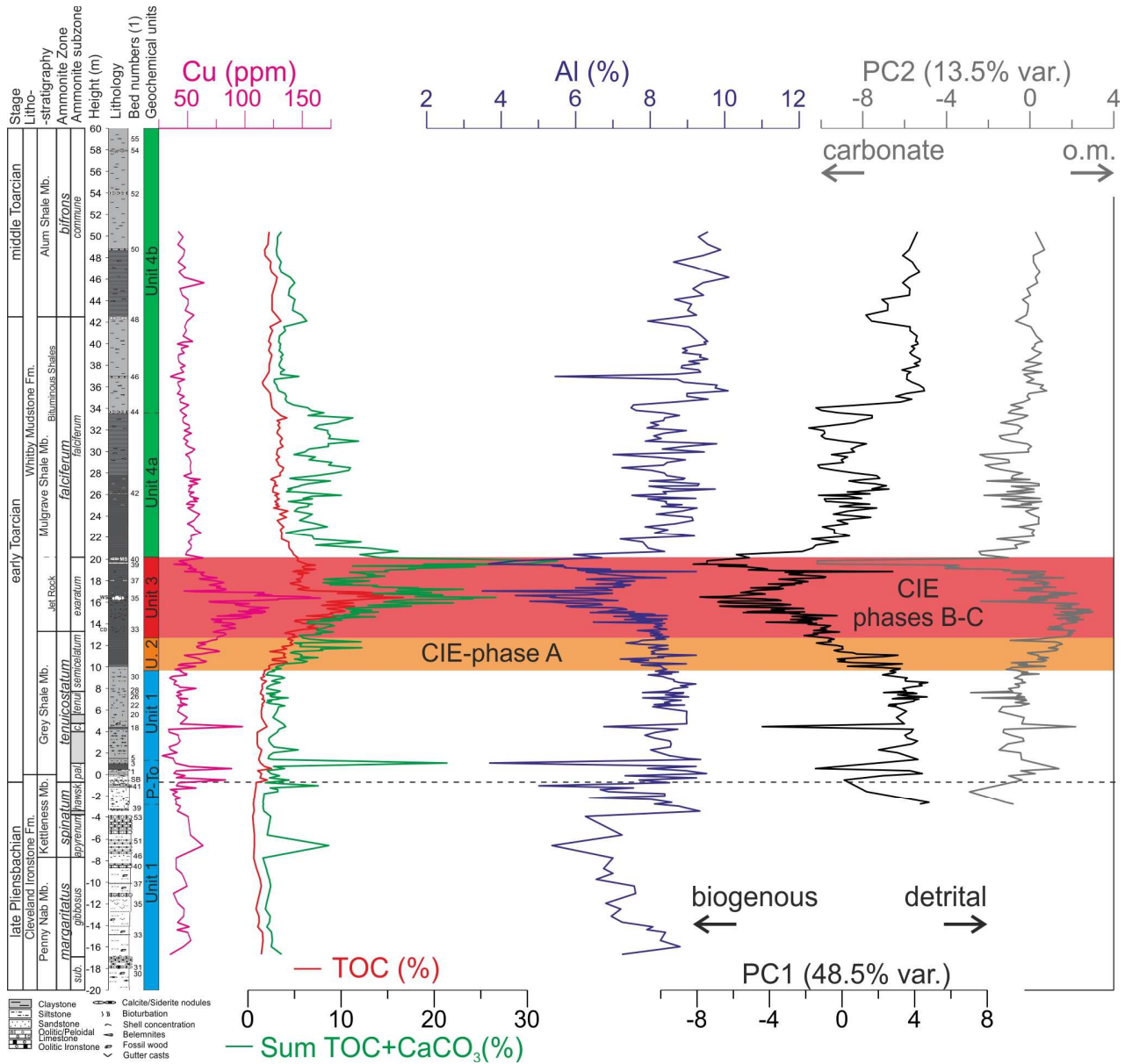
11

Figure 5: Comparison of trends observed in %TOC and %CaCO₃, Al and Cu concentrations to trends observed in principal components PC1 and PC2. Al is taken here as the standard lithogenous element. (1) Bed numbers following **Howarth (2002)**.

4.3. Degree of pyritization

Data originated from the samples of the Cleveland Basin plot along a single line of regression in a S vs Fe crossplot with a slope of 1.4 %Fe and an intercept at -4.1 (Fig. 7A). The strong co-variation indicates a clear relationship between the two elements, as previously noted by **McArthur et al. (2008)**. The negative intercept indicates an excess in Fe relative to sulphur, which suggests that part of the Fe is not in the form of pyrite. Fe can thus be considered to be derived from two fractions, one non-

reactive fraction situated in detrital minerals and siderite, and a reactive fraction that tends to be available for pyritization. When Fe$_{pyrite}$ is substracted from total Fe, the remaining signal shows long-term trends that are similar to aluminosilicate elements such as Al, with the exception of a few positive peaks which are related to stratigraphic levels with siderite nodules (compare Fig. 5 and Fig. 8). The very strong correlation between total Fe and total S observed here, and the steepness of the slope which even exceeds that of the line of stoichiometric pyrite suggests that most of the available reactive Fe was pyritized and that the only limiting factor for pyritization was thus the available amount of S. It also shows that a vast amount of the available sulphur has been incorporated into pyrite. This observation lends further support to the calculation and use of a "degree of pyritization" proxy (DOP-T) based on a simple ratio of (total S)/(total Fe), as in **McArthur et al. (2008)**.
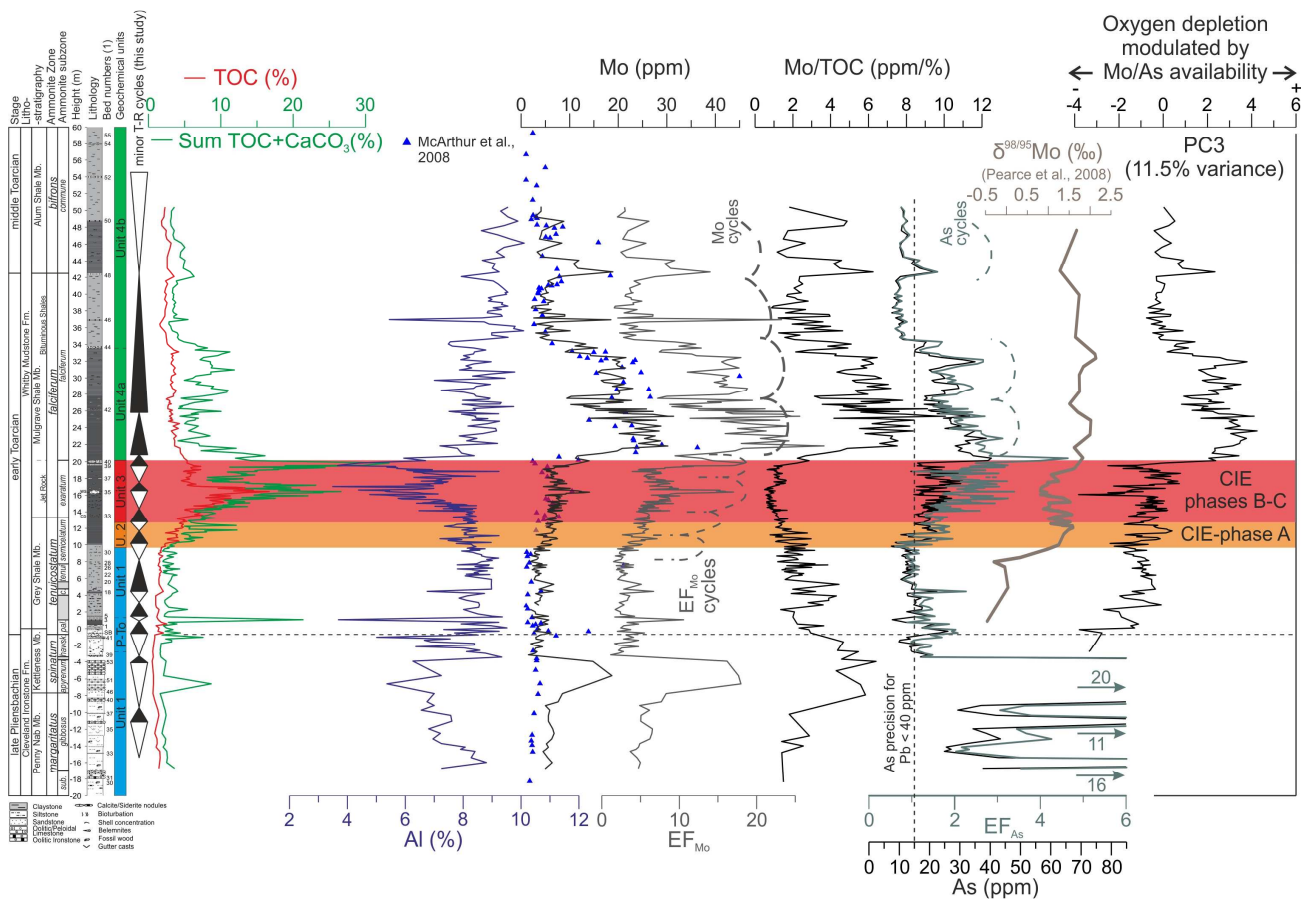

Figure 6. %TOC and %CaCO$_3$, Al, Mo and As concentrations, enrichment factors (EF) in Mo and As, Mo/TOC, $\delta^{98/95}$Mo, and principal component PC3. A number of redox cycles are tentatively drawn based on EF$_{Mo}$ across the CIE interval (units 2 and 3) and based on common trends in Mo and As concentrations above the CIE (unit 4). (1) Bed numbers following **Howarth (2002)**.

Samples that plot between DOP-T lines of 0.5 to 1 (Fig. 7A) may be considered as deposited under conditions of increasing oxygen deficiency from anoxic to euxinic conditions when adopting the framework erected on the basis of geochemical data from shale of the Upper Pennsylvanian Kansas-

Type cyclothems (**Algeo and Maynard, 2004**). In contrast, samples that plot between DOP-T lines of 0.25 to 0.5 may be considered as deposited under suboxic to dysoxic conditions and samples situated below the DOP-T line of 0.25 as deposited under oxic conditions (**Algeo and Maynard, 2004**). The degree of pyritization in the sediments is considered an excellent redox proxy indicating fluctuations in oxic conditions at the sea-floor (**Raiswell et al., 1988**). Trends and values of the DOP-T have previously been discussed by **McArthur et al. (2008)** and our data reproduce and refine these trends (Fig. 8). Very high DOP-T values of 0.8 to 0.9 in Units 2 and 3 (pre-CIE and CIE intervals) have been interpreted as attesting to long-term euxinic conditions in the Cleveland Basin and in the Posidonia Shale of NW Germany (**Raiswell and Berner, 1985**; **Wignall et al., 2005**; **McArthur et al., 2008**; **Pearce et al., 2008**), whereas values below 0.4 in Unit 1 and in Unit 4b indicate only oxic to anoxic conditions in the water column (Fig. 8).

4.4. Trace metals (Cu, Mo, As)

Some trace metals, e.g. Cu, Ni, Cr and Co, are considered to be of weak euxinic affinity (**Algeo and Maynard, 2004**). This attribution conveys an ambiguous relationship of these trace elements to TOC in the absence of a priori information regarding sedimentary redox conditions. Cu has been shown to exhibit two distinct slopes of correlation with TOC with a low slope in anoxic facies and a slightly steeper slope in euxinic facies (**Algeo and Maynard, 2004**). In our dataset, a close match is observed between trends of Cu and TOC as can be observed in Figure 2 and as expressed in the multivariate statistics (Fig. 4). Only one line of correlation can be highlighted here between Cu and TOC with a slope of 7 and a R^2 coefficient of correlation of 0.72. Therefore, this element has a limited use here to distinguish the degree of oxygen deficiency and/or basinal restriction.

In contrast, trace elements such as U, V, Zn, Pb and Mo have been considered to be of strong euxinic affinity, with high concentration and enrichment factors that positively deviate in euxinic facies from the line of correlation drawn for anoxic facies (**Algeo and Maynard, 2004**). Among these elements, Mo is by far the best studied and its behaviour in response to redox and hydrographic conditions has been well constrained (**Algeo, 2004**; **Algeo and Maynard, 2004, 2008**; **Algeo and Lyons, 2006**; **McArthur et al., 2008**; **Pearce et al., 2008**; **Hetzel et al., 2009**; **Algeo and Rowe, 2012**; **Berner et al., 2013**). As previously described by **McArthur et al. (2008)**, Mo increases only very slightly within the pre-CIE and CIE intervals whereas very high concentrations are reported in Unit 4, especially within the laminated black shales of Unit 4a (Fig. 6). Our high-resolution data allow for the potential recognition of four redox cycles in Mo enrichment factors (EF_{Mo}) across the pre-CIE and CIE intervals as well as 4 distinct cycles within Unit 4 (Fig. 6). The evolution of arsenic concentrations in the studied sequences exhibits trends similar to those of Mo (presented via As enrichment factors; EF_{As}), although the increase in As and in EF_{As} values within the pre-CIE and CIE intervals is much better defined than for Mo (Fig. 6). Cross-plots of Mo vs TOC and As vs TOC show remarkably similar trends but with distinct slopes of correlation between Unit 4 and Units 2-3 (Fig. 7C and 7E). The same observation is true for the Mo/TOC and As/TOC ratios vs DOP-T. Both graphs show that a significant correlation between the two tested parameters is restricted to Unit 4 (Fig. 7D and 7F).
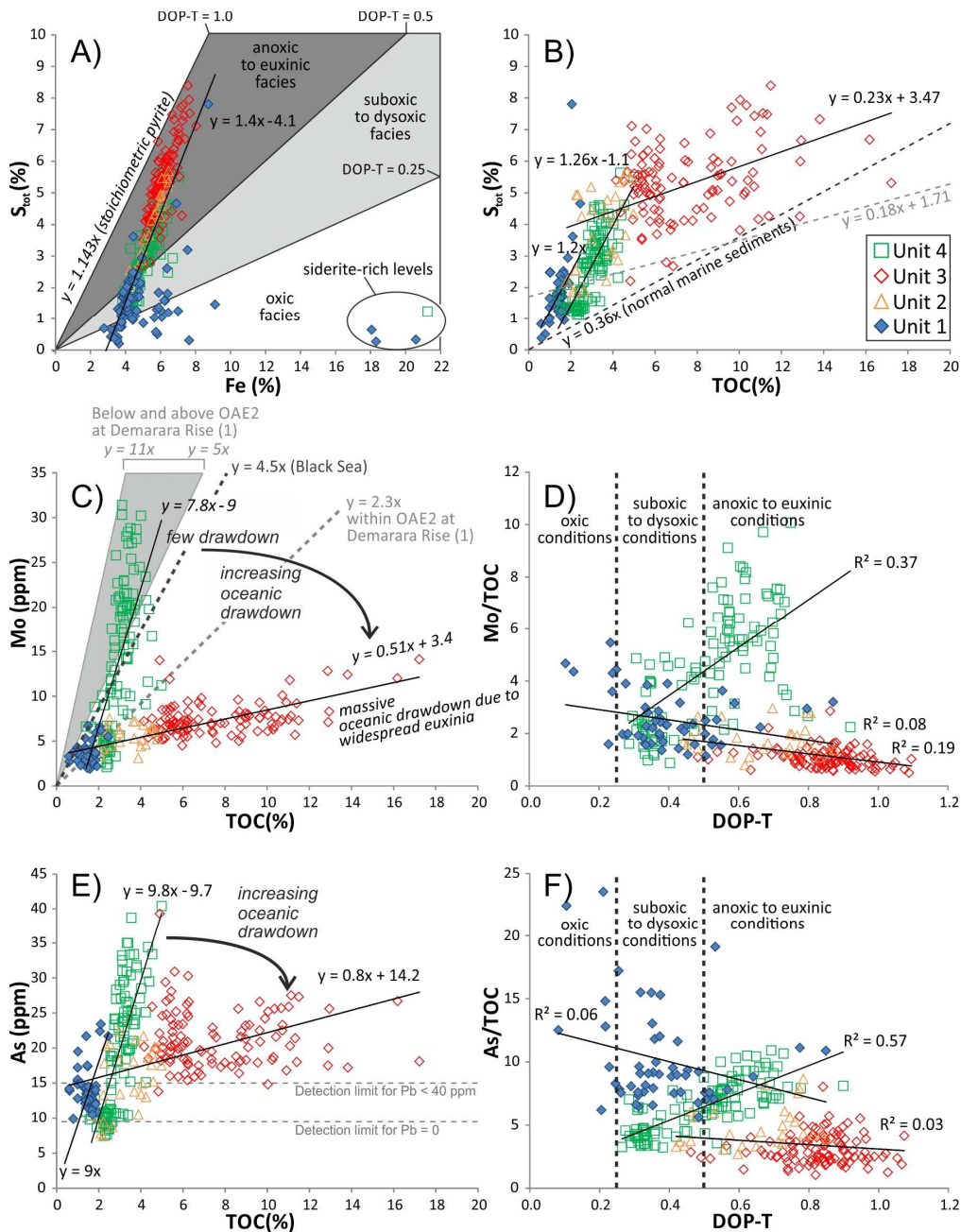
Figure 7: Various crossplots. A) S vs Fe, B) S vs total organic carbon (TOC), C) Mo vs TOC, D) Mo/TOC vs degree of pyritization based on total Fe (DOP-T), E) As vs TOC, F) As/TOC vs DOP-T. Siderite-rich levels have not been considered in graphs 7C to 7F. Values of the DOP-T at 0.25 and 0.5 and relationship to potential oxic to euxinic conditions are based on observations by **Algeo and Maynard (2004)**. Slopes and fields of Mo vs TOC values of Demerara Rise (1) are based on data from **Hetzel et al. (2009)** and reviewed by **Algeo and Rowe (2012)**. The slope of Mo vs TOC for the Black Sea is based **on Algeo and Lyons (2006)**. The slope of 0.36 for S/TOC of normal marine bottom-water conditions is from **Berner and Raiswell (1983)**. The slope and intercept of 0.18 and +1.71 for S vs TOC corresponds to the regression line calculated for sediments of the uppermost Tenuicostatum to Bifrons zones of the Posidonia shale in SW Germany (Weilstetten core, **Berner et al., 2013**).
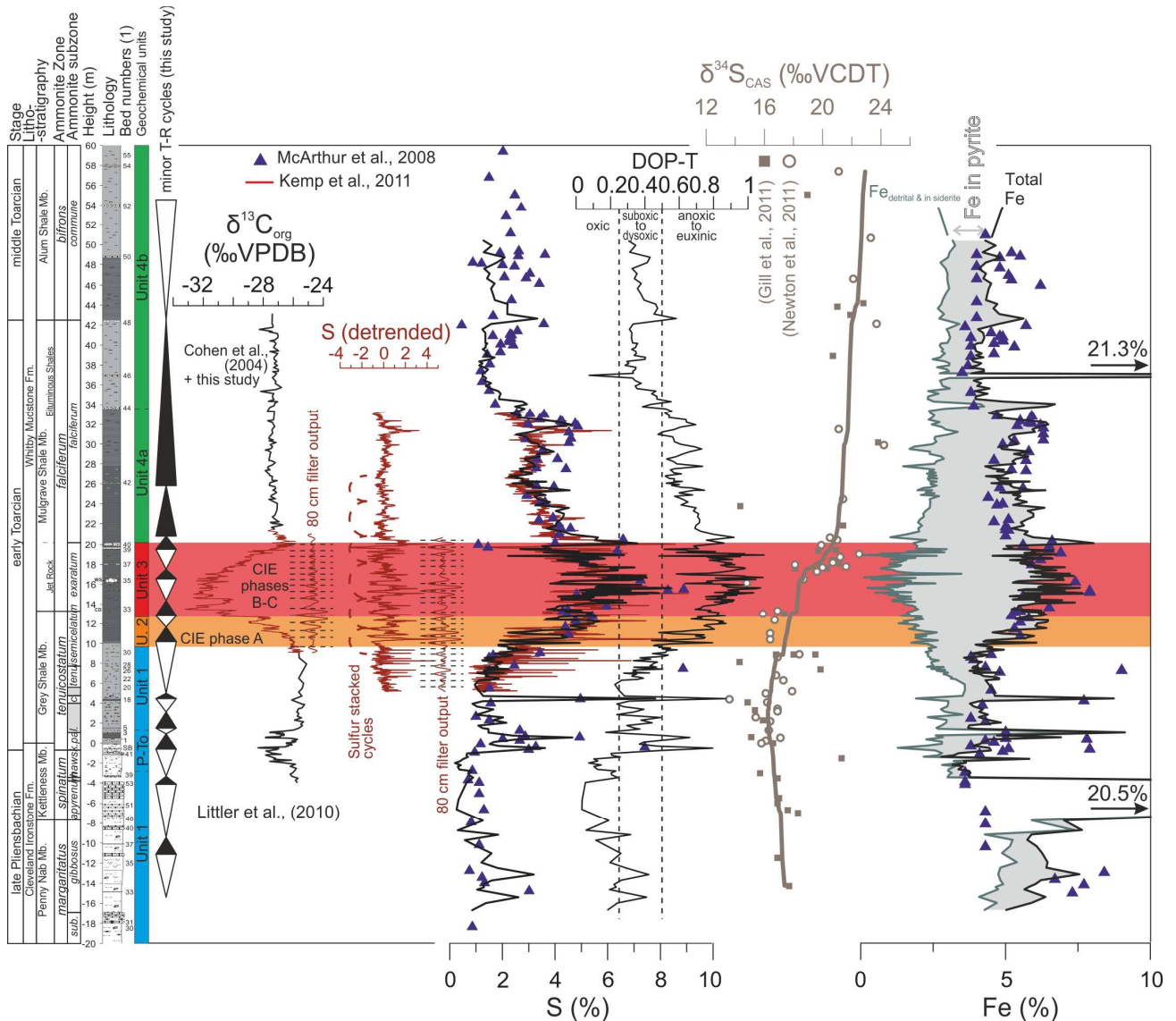
Figure 8: $\delta^{13}C_{org}$, Sulfur concentration with a 80 cm filter output, $\delta^{34}S$ data, degree of pyritization based on total Fe (DOP-T), and difference between total and non-reactive Fe (detrital and in siderite). (1) Bed numbers following **Howarth (2002)**.

5. Discussion

5.1. Stratigraphic subdivision, correlation and duration of the early Toarcian CIE

Carbon isotopes have now become a standard chemostratigraphic tool for global-scale stratigraphic correlation throughout the Precambrian and Phanerozoic (**Saltzman and Thomas, 2012**). Transient carbon isotope excursions, either positive or negative, have proven useful in correlating synchronous sedimentary sequences that record global perturbations in the exogenic carbon cycle. However, in contrast to other non-geochemical tools, carbon-isotope stratigraphy suffers from the lack of a formalized methodology to correlate excursions tied by biostratigraphy. Carbon-isotope stratigraphy is particularly well proved for the early Toarcian, but the occurring CIE has been subdivided and defined

16

in contrasting ways (**McElwain et al., 2005**; **Hesselbo et al., 2000, 2007**; **Kemp et al., 2011**; **Hermoso et al., 2012**; **Boulila et al., 2014**; **Bodin et al., 2016**; **Boulila and Hinnov, 2017**). Some authors have used the cyclic nature of the initiation and lower half of the negative CIE to define distinct steps (**Kemp et al., 2011**; **Hesselbo and Pienkowski, 2011**; **Hermoso et al., 2012**). Others have focused on attempting to define the "onset" and "termination" of the CIE and subdivide the negative excursion into falling and rising limbs (**Kemp et al., 2011**; **Boulila et al., 2014**; **Boulila and Hinnov, 2017**) or defined distinct intervals or lines of correlation based on distinctive features in the shape of the curve (**Hesselbo et al., 2000, 2007**; **Kemp et al., 2005**; **McElwain et al., 2005**; **Bodin et al., 2016**). The various subdivisions used in the literature result in confusion and correlation uncertainty, and also hampered the vivid ongoing debate on the duration of the CIE based on astronomical forcing of physical, chemical and biological proxies in sedimentary records (**Kemp et al., 2005, 2011**; **Suan et al., 2008**; **Boulila et al., 2014**; **Huang and Hesselbo, 2014**; **Ruebsam et al., 2014, 2015**; **Martinez et al., 2017**; **Boulila and Hinnov, 2015, 2017**). In a recent review on the duration of the Toarcian negative CIE, **Boulila and Hinnov (2017)** subdivided the CIE in two distinct intervals: the decreasing part (DP) and increasing part (IP) with a base of their DP interval situated at what they consider as the "onset" of the CIE, which happens to correspond to the onset of well-expressed sedimentary cyclicity (Fig. 9). Although this stratigraphic subdivision may be viable in terms of palaeoceanographic and palaeoenvironmental change, the position of the onset of the CIE may be poorly defined, because the Toarcian carbon isotope record is, in many records, characterised either by a low-amplitude, cyclic progressive decrease, by a steady cyclic trend, or sometimes even by a slight increase in the upper half of the Tenuicostatum or Polymorphum zones (see Fig. 11 of **Bodin et al., 2016**). The onset of the Toarcian CIE is defined in different ways and is thus unlikely to represent a viable stratigraphic marker. Moreover, hiatuses have been characterised around the onset of the T-OAE in some marine basins (discontinuity D2 of **Pittet et al., 2014**).

An interval of low-amplitude, stepwise, progressive decreasing values in $\delta^{13}C_{org}$ is defined here as phase A of the CIE at Hawsker Bottoms (Fig. 9). In contrast, an initial abrupt negative carbon isotope shift appears to be a recurrent feature of the CIE, occurring nearly in coincidence with the base of the Levisoni Zone in Portugal and Morocco, and 60 cm below the base of the Falciferum Zone at Yorkshire coastal outcrops (Fig. 9, **Bodin et al., 2016**). Even though it cannot be excluded that local controls have significantly altered the expression of the CIE and thus its onset, this initial abrupt shift is considered here as one of the most reliable chemostratigraphic markers for correlation and is used to define the base of phase B of the CIE (Fig. 9). Phase B corresponds to an extended interval representing the isotopically lighter values. Separating the CIE into a falling and rising limb is a perilous task for detailed stratigraphy of the Toarcian OAE as it implies the unambiguous recognition of a globally, correlatable, narrow stratigraphic interval where carbon isotope values reach a minimum. Such a narrow interval can be recognised from the bulk carbonate $\delta^{13}C$ values, but not in the bulk organic carbon-isotopes of the Sancerre-Couy core (**Hermoso et al., 2012, Peti et al., 2017**), the latter showing a variability of <1 ‰ in a 1.5 m thick interval (Fig. 9; **Hermoso et al., 2012, Peti et al., 2017**). Also, the $\delta^{13}C_{org}$ of Yorkshire and the bulk carbonate carbon-isotope record of Peniche show the lightest values with minor variability over an interval of several metres (Fig. 9). The upper boundary of phase B has thus been defined here by the last local minimum preceding a rise in carbon isotopes (Fig. 9). This subsequent rise is stratigraphically abrupt in the Sancerre-Couy core, suggesting condensation, but more gradual at Yorkshire and Peniche (Fig. 9). Phase C of the Toarcian CIE corresponds to the unambiguous rising limb of the $\delta^{13}C$ curve and ends with the stratigraphically confined $\delta^{13}C_{org}$

maximum, often (but not always) expressed by a small bulge (Fig. 9). Phase A corresponds to geochemical Unit 2 whereas phases B and C correspond to geochemical unit 3 (Fig. 2, Fig. 9).
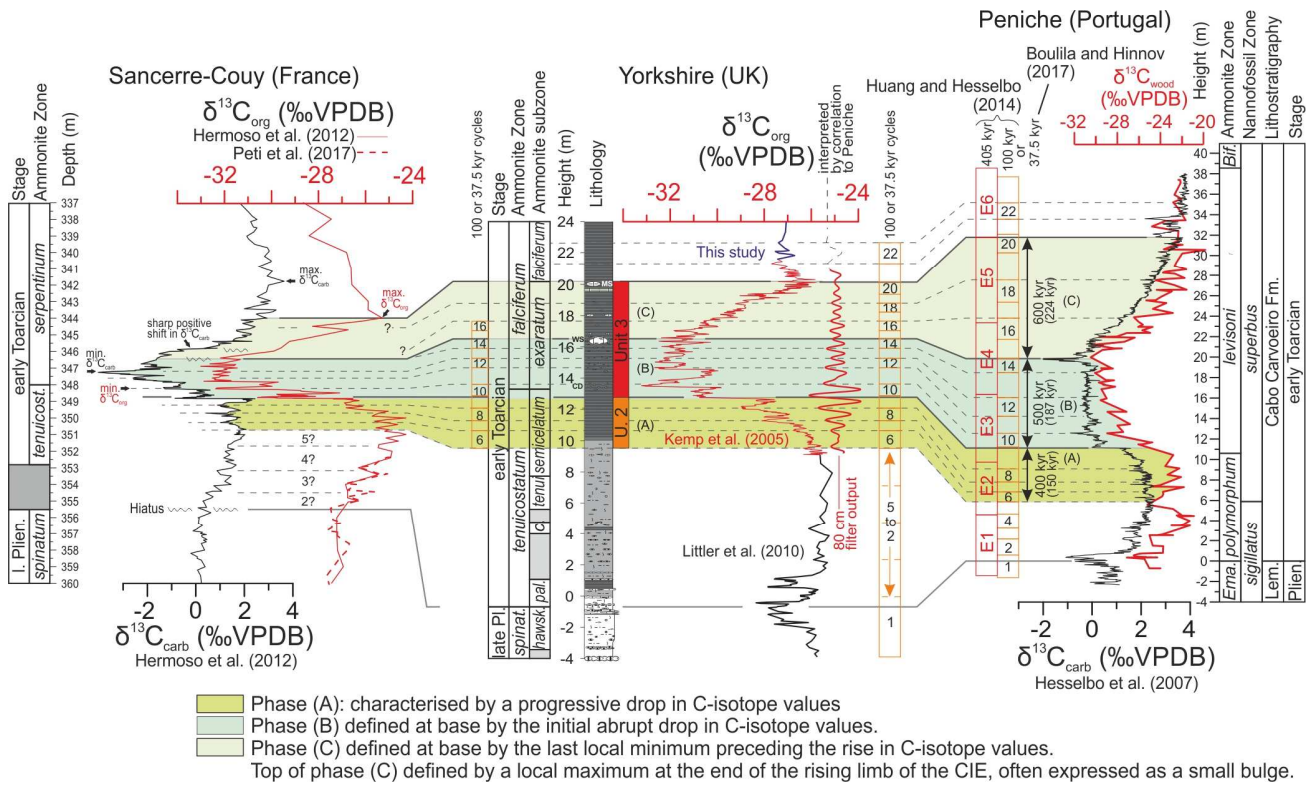

Figure 9. Correlation of the P-To event and Toarcian CIE between Sancerre-Couy (Paris Basin), Yorkshire and Peniche (Portugal) at the scale of the cycles identified by **Huang and Hesselbo (2014)**. Note that **Boulila and Hinnov (2017)** tuned their obliquity signal to 35 kyr whereas duration of 37.5 kyr for obliquity was chosen here following **Waltham (2015)**.

The duration of the T-OAE is the subject of controversy (**McArthur et al., 2000, 2016**; **Kemp et al., 2005, 2011**; **Suan et al., 2008**; **Boulila et al., 2014**; **Huang and Hesselbo, 2014**; **Ruebsam et al., 2014, 2015**; **Martinez et al., 2017**; **Boulila and Hinnov, 2015, 2017**). Besides the use of ambiguous stratigraphic subdivisions of the CIE of some authors, this controversy mostly relates to the predominance of essentially one significant periodical component in various proxies of phases A to C of the CIE. This feature is particularly pronounced for the sedimentary records of the Cleveland Basin where only a 75 to 80 cm cyclicity in $\delta^{13}C_{org}$, S and TOC data could be confidently recognized as a potential Milankovitch component in cyclostratigraphic analyses (**Kemp et al., 2005, 2011**). In our new high-resolution XRF data, the 75 to 80 cm cyclicity of **Kemp et al. (2005, 2011)** is not detected (Fig. 2B). However, a distinct 350 cm cyclicity in Zr/Al, Si/Al, and particularly well-pronounced in Zr/Rb can be highlighted in the LOWSPEC spectrum above the 95% confidence level (Fig. 2B). High-frequency cycles also appear significant at 37 and 29 cm above the 95% confidence level, 22 and 17 cm above the 99% confidence level (Fig. 2B). Four of the ~3.5 m thick cycles span phases A to C of the CIE (Fig. 2). Variations in Mo also suggest 4 cycles in the same stratigraphic interval (Fig. 6). Ratios between the peaks at 29 and 37 cm to 350 cm suggest the relationship from obliquity to 405 kyr-

long eccentricity, while peaks at 22 and 17 cm would match well with the precession. In addition, comparison of the 350 cm filter output of Zr/Rb to a 80 cm filter output of $\delta^{13}C_{org}$ original data of **Kemp et al. (2005)** suggests an average ratio of 4.4 between these two periodical components. Such a ratio points to average periodicities of 165 and 440 kyr when considering the 80 cm cycles as driven by obliquity (37.5 kyr at 182 Ma according to **Waltham, 2015**) as in **Kemp et al. (2005)** or 100 kyr short eccentricity as in **Huang and Hesselbo (2014)**, respectively. Neither of these two durations allows for a definite settlement of the duration controversy, though we note that the short-eccentricity interpretation of **Huang and Hesselbo (2014)** for the 80 cm cycles would mean that the 3.5 m cycles, if of astronomical origin, are in close agreement to the 405 kyr-long eccentricity.

Correlation of the three T-OAE successions that present high-resolution isotope data is presented in Figure 9. Regardless of the nature of the cycles suggested for the three localities (obliquity, **Boulila and Hinnov, 2017** vs short-eccentricity, **Suan et al., 2008**; **Huang and Hesselbo, 2014** and **Martinez et al., 2017**), a cycle to cycle correlation can be performed between Peniche, Yorkshire and Sancerre-Couy by adopting the numbering of the putative eccentricity cycles of **Huang and Hesselbo (2014)**. This correlation shows a good match between cycle 6 (base of phase A) and 13 in all localities and between 6 and 22 for Peniche and Yorkshire. This correlation is straightforward when using the first abrupt $\delta^{13}C$ decline in carbonate and organic matter (base of phase B) as the main "tie point" (Fig. 9). However, the correlation at the top of the Tenuicostatum Zone between Sancerre-Couy and Yorkshire is less straightforward and depends on the carbon source considered ($\delta^{13}C_{org}$ vs. $\delta^{13}C_{carb}$). For instance, the most negative value in $\delta^{13}C_{carb}$ at Sancerre-Couy is situated within the lower Serpentinum Zone, suggesting that it may not be stratigraphically correlative with the first local minimum in $\delta^{13}C_{org}$ at the base of the Exaratum Zone at Hawsker Bottoms (Fig. 9). Rather, this first local minimum in $\delta^{13}C_{org}$ at Hawsker Bottoms seems to correspond to the first distinctive local minimum in $\delta^{13}C_{org}$ situated immediately below the very top of Tenuicostatum Zone at Sancerre-Couy (Fig. 9), a view that is similar to the correlation between Peniche and Sancerre-Couy recently proposed by **Bodin et al. (2016)**. Similarly, the maxima in $\delta^{13}C_{org}$ and $\delta^{13}C_{carb}$ at the top of the recovery phase of the CIE in Serpentinum do not coincide at Sancerre-Couy (Fig. 9). A similar situation occurs at Peniche (Fig. 9) and Rietheim with maxima of the $\delta^{13}C_{org}$ preceding the maxima in $\delta^{13}C_{carb}$ by several meters (**Hesselbo et al., 2007**; **Montero-Serrano et al., 2015**). While correlating the CIE, it is therefore recommended to use the same carbon source, an exercise that is achieved here focusing on the correlation of $\delta^{13}C_{org}$ patterns between the three sections (Fig. 9). Using the cyclic framework proposed for the Peniche succession by **Huang and Hesselbo (2014)**, the 80 cm filter output of $\delta^{13}C_{org}$ at Hawsker Bottoms, and the potential expression of these cycles in phases A and B of the $\delta^{13}C_{org}$ record of Sancerre-Couy, a detailed correlation of the three sections is possible and highlights condensation at Sancerre-Couy within phase C (Fig. 9). This correlation shows that the sharp positive recovery in $\delta^{13}C_{org \ and} \ \delta^{13}C_{carb}$ data of Sancerre-Couy at 345.7 m corresponds to a gradual carbon isotope increase in Yorkshire and at Peniche. Thus, a number of the cycles identified in the two latter sections are not or poorly pronounced at Sancerre-Couy (Fig. 9). This resulting interpretation advocates against the use of the Sancerre-Couy core as a reliable sedimentary archive for estimating the duration of the Toarcian CIE. Nevertheless, likely durations of the 3 distinct phases of the CIE are suggested here based on the recognition of distinct periodicities in proxy-records from Hawsker Bottoms and Peniche, following the short-eccentricity (100 kyr) and obliquity (37.5 kyr) hypothesis (Fig. 9).

5.2. Lithogenic elements and relative sea-level change

Previous sequence stratigraphic appraisals of the upper Pliensbachian to mid-Toarcian succession in the Cleveland Basin suggest that a comparatively low sea-level characterised the upper Pliensbachian with sea-level drops corresponding to the uppermost Margaritatus Zone and at the Pliensbachian-Toarcian boundary (**Wignall et al., 2005**; **Hesselbo, 2008**; **Powell, 2010**). For the studied part of the Toarcian, a sustained transgression occurred interrupted only by a minor short-term relative sea-level drop in the latest Tenuicostatum Zone (**Hesselbo, 2008**).

The main lithogenic elements, including Si, Ti, K, Rb and Zr, expressed as elemental/Al ratios (**Chester et al., 1977**; **Pye, 1987**), are tested as complementary proxies for relative sea-level change, as they reflect changes in clastic transport due either to variations in the proximity of the siliclastic source, or, alternatively, changes in continental run-off due to modifications of the hydrological cycle. Also Cr, used as a redox proxy (**Tribovillard et al., 2006**), appears to be mainly of detrital origin in the Toarcian of the Cleveland Basin, showing a similar behaviour to lithogenic elements. All these elements (except K) show similar trends, are found in the same geochemical cluster (Fig. 4), and oppose the biogenic and hydrogenic elements in PC1 (Figs 3–4). In particular Si/Al, Zr/Al and Zr/Rb show nearly the exact same trends, suggesting coincident changes in the fluvial transport of siliciclastics and in clastic grain size (Fig. 2). Such coincidence suggests that the grain-size variations expressed by Zr/Rb primarily reflect distance from the clastic source (**Liu et al., 2004**; **Chen et al., 2006**; **Aquit et al., 2016**). These three proxies may thus be interpreted in terms of proximity of the detrital source.

Element/Al ratios show strong enrichments in the uppermost Pliensbachian, followed by a progressive decrease up to the top of the Exaratum Subzone (including numerous minor cycles of variable amplitudes) and subsequent relatively stable ratios throughout the remainder of the studied interval (Fig. 2). The similarity of these lithogenic element ratios with Si/Al suggests that most of the silicon is detrital in origin, and that biogenic silica is negligible. The different trends observed in K/Al (not shown here) as compared to other ratios in detrital proxies, may be due to significant changes in the clay mineral composition (**Boyle, 1983**; **Weaver, 1967, 1989**; **Niebuhr, 2005**).

The long-term trends of Zr/Rb, Zr/Al and Si/Al match well with the relative sea-level curve inferred on the basis of visual observations in the field (**Hesselbo and Jenkyns, 1998**; **Hallam, 2001**; **Hesselbo, 2008),** and higher-order cyclic changes in these three elemental ratios allow for the detection of a number of detrital cycles that are on the scale of 3–4 m thick parasequences hitherto undescribed form the Yorkshire section (Fig. 2). These dominant coarsening upward clastic cycles show distinct so-called stacking patterns, i.e. progressive change in character up-section. In figure 2 we identify a backstepping stacking pattern in the lowermost Toarcian strata reaching a peak at about the middle of the Tenuicostatum Zone, followed upward by a slight progradation to the mid Semicelatum Subzone, and then a backstepping pattern through the entire CIE to the top of the Exaratum Subzone (top of the Jet Rock) where silt sized clastic content presumably diminishes to zero (Fig. 2).

Comparisons with inferred relative sea-level trends in the Sancerre-Couy succession may be instructive (Fig. 10). We note that, at first sight, the interpretation of the Yorkshire sequence is in conflict with that at Sancerre-Couy, where **Hermoso et al. (2013)** recognise a regressive trend through the whole CIE interval. The Sancerre-Couy relative sea-level change interpretation is based principally on

Quartz/(Quartz+Clay) as determined by whole rock XRD (**Hermoso et al., 2013**). However, in contrast, the Zr/Al ratios through the same interval show, if anything, a trend toward lower ratios – i.e. what would be expected from an upward fining trend to less silt-sand rich strata, and remarkably similar to the observed pattern in the same elements from Yorkshire (Fig. 2). This contrast in proxy trends suggest the possibility that at Sancerre-Couy, either the Quartz/(Quartz+Clay) ratio is affected by occurrence of diagenetic silica in the upper parts of the OAE record, or that the ratios are misleading because of highly variable dilution by carbonate phases, or both. This assertion is supported by the mean carbonate concentrations recorded at Sancerre (between 20 and 60%) compared to those recorded in Yorkshire (mostly below 20%). Further SEM-based observations on the Sancerre-Couy sediments are required to resolve these issues.
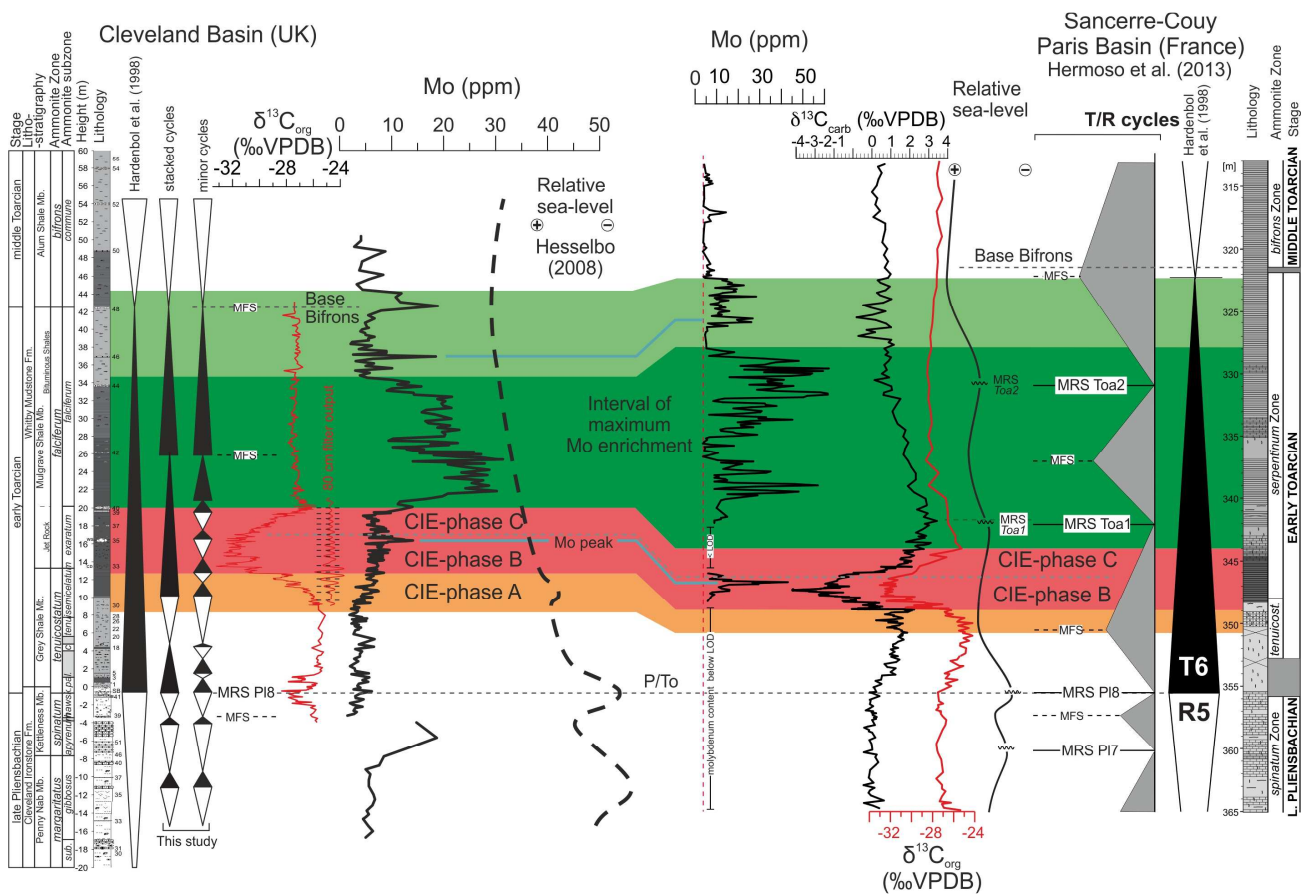

Figure 10. Correlation of sequence stratigraphy, carbon isotopes and Mo trends between Sancerre-Couy (Paris Basin) and Yorkshire (Cleveland Basin).

If the 80 cm filter output of $\delta^{13}C_{org}$ data is assumed to represent 100 kyr cycles, then the four ~3.5 m detrital cycles depicted across the CIE, may indicate the presence of a long-term astronomical control on sea level (possibly, ~405 kyr eccentricity cycles), in-line with independent evidence from the Jurassic and Cretaceous (e.g. **Gale et al., 2002**; **Huang et al., 2010**; **Sames et al., 2016**). These results would also point to a total duration of the CIE of c. 1.5 Myr (~15 cycles of 100 kyr and ~3.5 cycles of 405 kyr spanning phases A to C, Fig. 9).

5.4. Degree of oxygen deficiency and/or of basinal restriction
5.4.1 Degree of pyritization
The degree of pyritization (DOP; Figs. 7, 8) has been interpreted to be a good proxy for the degree of oxygen deficiency in bottom waters within the Cleveland Basin (**McArthur et al., 2008**; **Berner et al., 2013**). Geochemical data suggest that shallow-water facies in the sediments of the upper Pliensbachian were deposited mostly under oxic conditions, but the presence of DOP-T values between 0.25 and 0.5 may point to anoxic conditions already within Unit 1 (Fig. 7D). The presence of sulphur bands and strong anomalies in Fe concentrations due to a large amount of siderite within a few restricted intervals of the upper Pliensbachian in Unit 1, however, hinder the strict application of oxygenation indices presented in Figure 7A and 7D. The Paltum and Clevelandicum subzones including the P/To boundary and the lower half of the Tenuicostatum Zone are then characterized by high-frequency fluctuations of the DOP-T. Values above 0.5 in three samples which are associated with laminated facies point to alternating oxic and anoxic conditions in this interval (Fig. 8). A progressive rise of the DOP-T with values above 0.3 characterizes the Tenuicostatum and the lower half of the Semicelatum subzones, indicating anoxia and progressing oxygen deficiency prior to phase A of the CIE. The high values in Units 2 and 3 (phases A to C of the CIE) suggest that these intervals were deposited under euxinic conditions (Fig. 8). However, values above 0.5 in the DOP-T of Subunit 4a may also suggest euxinic conditions succeeding the Toarcian CIE in the Cleveland Basin (**McArthur et al., 2008**). Values of DOP-T fall mainly into the range of 0.3 to 0.5 within Subunit 4b, pointing to anoxic conditions in this interval. Trends in the DOP-T may appear, at first sight, to be in contrast with the $\delta^{34}S$ of carbonate-associated sulphate ($\delta^{34}S_{CAS}$), which shows a positive excursion with an onset within phase C of the CIE (Fig. 8). This positive excursion has been related to a globally significant perturbation in the sulphur cycle under anoxic conditions when microbial sulphate reduction, resulting in widespread pyrite formation, was the dominant biological process in seawater (**Gill et al., 2011**; **Newton et al., 2011**). However, this excursion occurs much later than the significant increase in pyritization highlighted by trends in the DOP-T (Fig. 8). This observed delay in the response of the sulphur cycle to widespread anoxia has been interpreted to reflect the long residence time of sulphate in the ocean (13–20 Myr in the modern ocean, **Berner and Berner, 1996**; **Gill et al., 2011**; **Newton et al., 2011**).

5.4.2 Molybdenum
The behaviour of Mo and its relationship with TOC in euxinic conditions (Fig. 7C) has allowed for the distinction of two distinct models of basin restriction in the Cleveland Basin (**McArthur et al., 2008**; **Pearce et al., 2008**; **Algeo and Rowe, 2012**). An abrupt rise in $\delta^{98/95}Mo$ at the base of the pre-CIE interval has been interpreted as the onset of the T-OAE and fast expansion of oxygen deficiency (**Pearce et al., 2008**). Rapid fluctuations of this proxy within the CIE interval (**Dickson et al., 2017**) indicate repetitive expansion and contraction of euxinia in the basin. Uniformly high Mo isotope ratios in our geochemical Unit 4 indicate regional anoxia to euxinia (Fig. 6). In contrast, sedimentary Mo-concentrations are not very high in phases A to C of the CIE and only increase significantly following the termination of the CIE (Fig. 6). These features have been explained by a significant drawdown of the trace-metal inventory of seawater through increased rates of Mo transfer to the basinal, or global, sedimentary reservoir, during an episode of widespread oceanic euxinia and/or strong basinal restriction (**McArthur et al., 2008**; **Pearce et al., 2008**; **Algeo and Rowe, 2012; Dickson et al., 2016, 2017**).

According to **McArthur et al. (2008)**, a shallow sill may have limited deep-water renewal, expansion of the pycnocline towards shallow depth, and organic matter and trace metal burial over a significant portion of the basin, depleting redox-sensitive trace metals from the basinal sea-water inventory. Increased organic sedimentation and a reduced Mo inventory in highly restricted environments result in a relationship of these two proxies with a low slope (Fig. 7C). In contrast, sediments deposited in euxinic conditions within a weakly restricted basin, and/or with frequent deep-water renewal show a much steeper slope for this correlation (Fig. 7C). A well-established example for this behaviour is reported from the Cenomanian-Turonian OAE2 at Demerara Rise (central Atlantic) (Fig. 7C, **Hetzel et al., 2009**; **Algeo and Rowe, 2012**). The slope of the Mo versus TOC regression observed for geochemical Unit 4 in the Yorkshire coastal outcrops compares well with the field of slopes observed below and above OAE2, indicating euxinic conditions in a weakly restricted basin. Therefore, the slope of 0.5 obtained for the Toarcian CIE interval (Units 2 and 3) would tend to suggest euxinic conditions with a strong restriction, relative to the observed slope of 2.3 defined within OAE2 (Fig. 7C). A direct consequence of the aqueous drawdown of Mo is the absence of correlation between the Mo/TOC ratio and DOP-T for sediments deposited within Units 2 and 3 (Fig. 7D). In contrast, a significant correlation exists between the two parameters in sediments from Unit 4, suggesting deposition under conditions of weak basinal restriction or more frequent deep-water renewal (Fig. 7D). In a recent study by **Goldberg et al. (2016),** which focused on the Cenomanian-Turonian boundary (OAE2), the expansion of euxinic bottom waters across large parts of the global ocean during OAE2 was sufficient to enhance a massive drawdown of Mo without any need for basin restriction. Goldberg and colleagues brought strong arguments showing that deep-waters of the proto-North Atlantic Ocean were only partially restricted and that this restriction cannot account for the patterns observed in Mo/TOC ratios. Therefore, the massive drawdown of Mo at times of oceanic anoxic events may only reflect the large scale and expansion of marine deoxygenation (**Goldberg et al., 2016**; **Dickson et al., 2016, 2017**). Differences in the Mo/TOC slopes obtained for OAE2 and the T-OAE could thus simply reflect the extent of the global seafloor area that was affected by deoxygenated water masses, and point to the T-OAE being of a much larger scale.

Stratigraphic correlation between the Sancerre-Couy core and the Toarcian sedimentary sequences of Yorkshire shows comparable trends in sedimentary Mo-concentrations (Fig. 10). The Posidonia shale in NW Germany also appears to show similar trends in Mo within and above the CIE (**Berner et al., 2013**; **Dickson et al., 2017**), suggesting a similar evolution of the Mo inventory in the Paris, Cleveland and Lower Saxony basins. The stacking pattern of the minor transgressive-regressive (T-R) cycles interpreted from the trends in our proxies of sea-level change (Zr/Al, Si/Al and Zr/Rb) clearly point to a stacked transgressive trend across phases A to C of the CIE, in contrast to the interpretation proposed for the Sancerre-Couy succession (Fig. 10).

The development of the C_{org}-rich, laminated facies across the T-OAE have been traditionally associated with a global marine transgression (T6 in Fig. 10, **Hermoso et al., 2013**); this is also suggested by marine influxes into continental (lacustrine) basins in China during the main phase of the T-OAE negative CIE (**Xu et al., 2017**). The sea-level interpretation at Sancerre suggests a potential match between the development of increasingly euxinic conditions and increased basinal restriction during phases A to C of the CIE, with a regressive trend in the Paris Basin that was terminated at the maximum regressive surface (MRS) Toa-1 (**Hermoso et al., 2013**), situated right at the top of the CIE (Fig. 10). However, this interpretation cannot be invoked for the Cleveland Basin which was, in

contrast, characterised at that time by a transgressive trend (Fig. 10). The "basin restriction" model thus appears to contrast with the relative sea-level trends in Yorkshire successions. Similarly to the recent interpretations drawn for OAE2, the basin restriction model does not appear to fit our observations of Yorkshire deposits. It is likely that the extreme environmental conditions that favoured the widespread development of euxinia during the T-OAE were enough to trigger a massive drawdown of Mo throughout the Boreal part of the peri-Tethys area as attested by the similar behaviour of Mo in UK, France and Germany.

5.4.3 Arsenic (As): a new critical element for the degree of oxygen deficiency and/or basin restriction in black shales?

Arsenic levels in the modern ocean, deep-sea and uncontaminated near-shore marine sediments range from 0.1 and 50 μg/g (**Maher and Butler, 1988**). Localized enrichment of arsenic is observed in the vicinity of mid-ocean ridges, where hydrothermal activity is a likely source for this element (**Elderfield, 1976**). Other anomalously high arsenic values in deep-sea sediments are associated with hydrothermal emanations (**Boström and Peterson, 1969**; **Boström and Valdes, 1969**). Sedimentary arsenic is mostly found in hydrous iron oxide phases and associated with sulphide minerals, such as M(II)AsS, where M(II) represents two-valent metals such as Fe, Ni or Co (**Maher and Butler, 1988**; **Matschullat, 2000**). Significant As enrichments are also observed in ferromanganese nodules (**Calvert, 1976**; **Maher and Butler, 1988**).

Solid-phase As levels in oceanic anoxic sediments are similar to those in oxic sediments today, although this element is likely associated with different mineral phases in these two types of sediments (**Calvert, 1976**; **Peterson and Carpenter, 1986**; **Maher and Butler, 1988**). A few studies have focused on the record of As in the geological record: Precambrian sediments appear to have been much richer in As prior to the oxygenation of shallow seas and Earth's atmosphere (**Sforna et al., 2014**) and As enrichment is associated with zones of pyrite crystals and aggregates in a limestone at the Cambro-Ordovician boundary of Sweden (**Vortisch et al., 1981**). Also, in Phanerozoic gold deposits, hosted in black shales and turbiditic sequences, arsenian pyrite causes As content of 10 to 200 μg/g and, rarely, up to 1,000 μg/g in bulk rocks (**Large et al., 2011**). Arsenic enrichment is thought to be related to co-deposition with organic matter in reduced continental margin deposits during periods of widespread oceanic anoxia, from which it is increasingly concentrated into arsenian pyrite during early diagenesis (**Large et al., 2011**).

Arsenic enrichment in black shales may therefore, arguably, be strongly associated with the degree of pyritization. The data presented here suggest a behaviour of As similar to that of Mo with As enrichments that exist only when the seawater inventory of this trace-metal is not affected by a massive drawdown (Fig. 6). Both elements correlate significantly with DOP-T only in Unit 4 (Fig. 7F) and exhibit a change of their element/TOC ratios from Units 2-3 to Unit 4 (Fig. 7E). A substantial drawdown of dissolved As from the seawater may thus be suggested for the CIE interval. However, a slight contrast in the trends of the two elements exists for the interval across the CIE. Here, EF_{As} shows a prominent increase, which is less obvious for EF_{Mo} (Fig. 6) and this may be explained by different oceanic residence times of the two elements (c. 100 kyr for As vs c. 730 kyr for Mo; **Faure, 1998**; **Algeo, 2004**). As suggested by the rapid fluctuations in $\delta^{98/95}$Mo within the CIE interval, euxinic conditions were likely interrupted by short episodes of deep-water renewal. Deep water ventilation may have been driven by storm events that have been interpreted to occur at a scale of c. 5 to 40 kyr

(**McArthur et al., 2008**). Such a renewal frequency would have been sufficient to replenish the basinal seawater inventory of As, whereas the basinal Mo inventory may have remained reduced.

This hypothesis opens interesting possibilities for comparing the behaviour of different trace metals across OAEs. For instance, V and Zn, which have short oceanic residence times (<50 kyr; **Faure, 1998**), behave similarly to Mo in the central Atlantic Ocean during OAE2 (**Hetzel et al., 2009**; **Algeo and Rowe, 2012**). The degree of drawdown and/or basin restriction in the juvenile Atlantic Ocean across OAE2 appears lower than that of the T-OAE in the Cleveland Basin when comparing their Mo/TOC slopes of regression (Fig. 7C). The similar behaviour of Mo, V and Zn may, however, indicate that deep-water renewal was strongly impeded throughout OAE2 at Demarara Rise whereas dissimilarities in the trends of these elements in Yorkshire advocates for frequent episodes of deep-water renewal. Documenting which trace metals show a drawdown across OAEs, related to their oceanic residence time, could potentially indicate the frequency of deep-water renewal.

5.5 Synthesis of sedimentary, biological and geochemical information

The well-exposed Toarcian black shales of Yorkshire have long been known and described (**Howarth, 1962** and references therein), and the significance of their lithology, mineralogy and trace and body fossil content have already been used for palaeoenvironmental reconstructions, long before any geochemical study was conducted (**Morris, 1979**; **Pye and Krinsley, 1986**; **O'Brien, 1990**). Changes in lamination style in particular have been related to the Toarcian transgression and benthic microbial mats, suggested to be responsible for wavy lamination in the interval spanning the Whale Stone to Millstone level, which encompasses phase C of the Toarcian CIE (**O'Brien, 1990**).

Trace fossil assemblages including *Chondrites* suggest oxic conditions in bottom waters and in the upper sediment layer during the lowest Toarcian Paltum Subzone up to the top of the Clevelandicum Subzone (**Morris, 1979**; Fig. 11). The sediments up to the top of geochemical Unit 1 (middle Semicelatum Subzone) are then characterized by a more restricted ichnofauna with dominant horizontal burrows, which gives way to an interval devoid of trace fossils that extends up to the top of the Falciferum Subzone (within Subunit 4b; **Morris, 1979**). Gradually more hostile bottom water conditions during deposition of the Jet Rock (Unit 3) are also reported in the re-appraisal of **Martin (2004)**. Horizontal burrows indicating the return to at least intermittently oxidising conditions in the top sediment layers only resume in the Commune Subzone (**Morris, 1979**). A similar sequence is observed for the diagenetic formation of carbonate nodules. Sideritic nodules are observed in the lower part of geochemical Unit 1 and in Subunit 4b, whereas pyritic calcareous concretions occur from the top of Unit 1 through to the lower part of Subunit 4b (**Morris, 1979**; **Pye and Krinsley, 1986**).

A progressive loss of benthic diversity goes alongside deteriorating bottom- water conditions and starts near the top of Unit 1 in the Semicelatum Subzone (**Harries and Little, 1999**; **Wignall et al., 2005**; **Caswell et al., 2009**; **Danise et al., 2015**). A clear benthic recovery is not observed within the studied interval (**Caswell et al., 2009**). Nektonic and nektobenthic animals were also affected by the T-OAE (**Harries and Little, 1999**; **Caswell et al., 2009**; **Ullmann et al., 2014**; **Danise et al., 2015**). In particular, a turnover in belemnites (**Harries and Little, 1999**; **Caswell et al., 2009**) and substantial changes in their isotopic composition in the Exaratum Subzone have been linked to bottom water anoxia, loss of benthic food resources and forced adaptations of belemnites from a nektobenthic to a nektonic life mode (**Ullmann et al., 2014**).
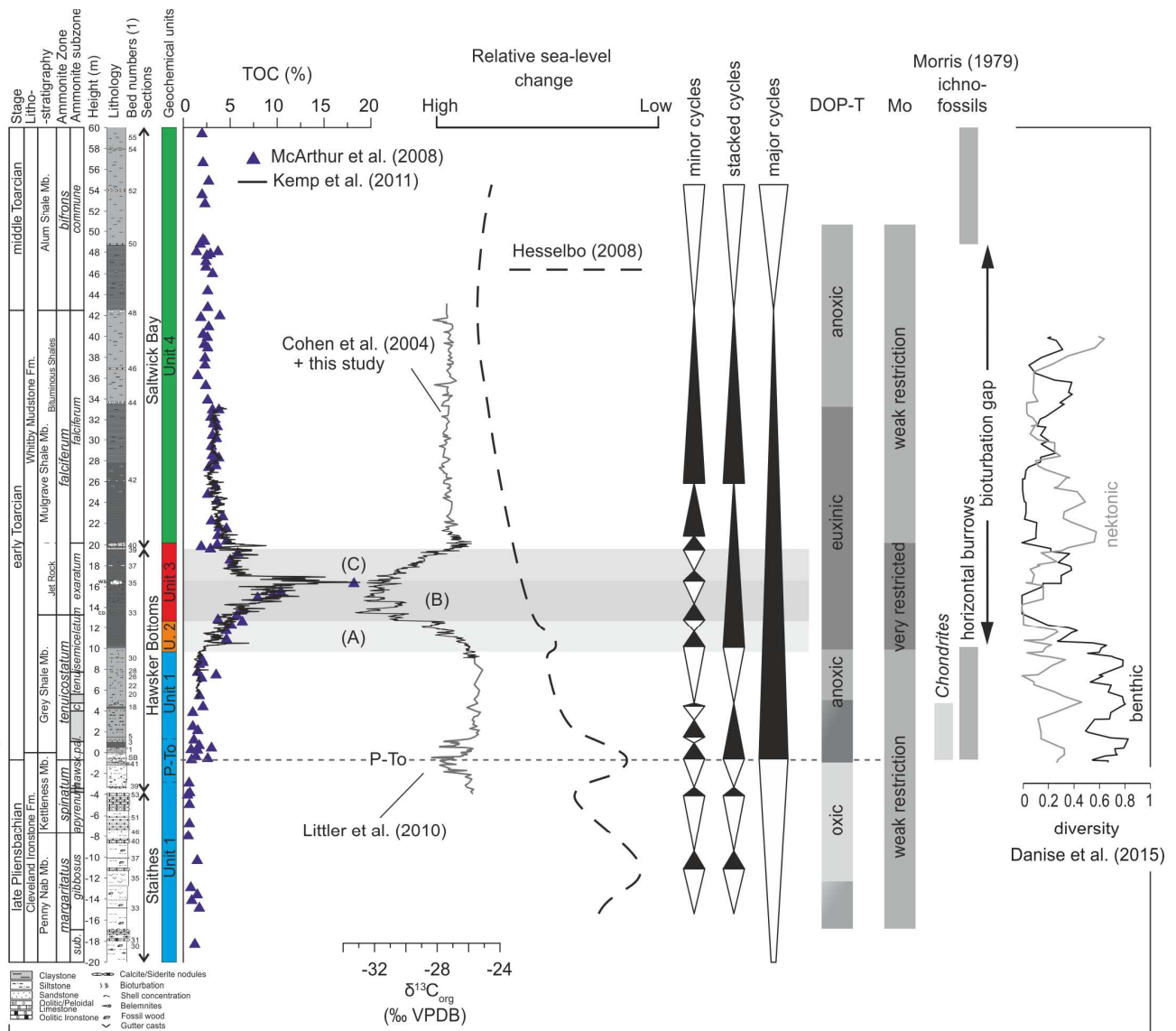
Figure 11: A summary of major environmental changes across the upper Pliensbachian to mid-Toarcian Yorkshire deposits (Cleveland Basin). (1) Bed numbers following **Howarth (2002)**.

Biological and sedimentological indicators of oxygenation tie-in well with geochemical proxies of water oxygenation presented here and in earlier studies (Fig. 11). This full array of data suggests that bottom water conditions and the sediment surface became inhospitable around the Semicelatum Subzone and that increasingly severe and long-lasting anoxia (and euxinia) led to the collapse of benthic biodiversity in the Exaratum and Falciferum subzones (Fig. 11). A slight amelioration of bottom water conditions is indicated from the base of the Falciferum Subzone onwards, where the DOP-T eventually indicates change from euxinic to anoxic conditions (Fig. 11), and some belemnite species seem to have intermittently migrated back to deeper waters (**Ullmann et al., 2014**). Only in the Commune Subzone, however, can an appreciable ichnofauna be observed again, indicating a return to

more oxygenated bottom water conditions, but benthic diversity did not fully recover within the studied interval up to the Commune Subzone, and the timing of the full recovery from longer-lasting deleterious effects on benthic organisms in Yorkshire has not yet been clearly depicted.

6. Conclusions

A new high-resolution major and trace-elemental geochemical dataset allowed for a review of the sedimentary expression of changing sea-level and oxygenation conditions across the P-To boundary and T-OAE. Detrital elements (Al, Si, Ti, Zr) have been used to draw a sequence stratigraphic framework for the Cleveland Basin. Four ~3.6 m cycles can be depicted from trends in detrital elements across the CIE, which may indicate the presence of a long-term astronomical control on sea level (possibly, ~405 kyr eccentricity cycles). These cycles occur in addition to the well expressed ~80 cm cycles previously documented in carbon isotopes, and which appear to be replicated in the carbon isotope records of other European sections. A cycle-to-cycle correlation of the CIE based on the short-term cycles expressed in carbon isotopes has been proposed between Yorkshire (UK), Peniche (Portugal) and Sancerre-Couy (France), highlighting the likelihood of hiatuses across the P-To and around the base of phase C of the CIE in France. C-S-Fe systematics and trace elements such as Mo and As of the Cleveland Basin highlight increasing anoxic conditions within the Tenuicostatum Zone, euxinia, strong water-mass restriction and/or maximum drawdown of a number of elements during the CIE, and a return to anoxic conditions within the upper half of the Falciferum Zone. Euxinia appears not to have been favoured in the Cleveland basin by water-mass restriction brought about by sea-level change which should, instead, have led to more open conditions at that time. The model of a "restricted" or "silled basin" to explain the major oceanic drawdown of elements such as Mo during the CIE suffers from a contradiction with sea-level trends in the Cleveland basin. By comparison to recent studies on OAE2, this drawdown may thus simply reflect the large expansion of bottom-water euxinia across the T-OAE.

References

Ahm, A.-S., Bjerrum, C.J., Hammarlund, E.U., 2017: Disentangling the record of diagenesis, local redox conditions, and global seawater chemistry during the latest Ordovician glaciation. Earth and Planetary Science Letters 459, 145–156, doi: 10.1016/j.epsl.2016.09.049.

Algeo, T.J., 2004: Can marine anoxic events draw down the trace-element inventory of seawater? Geology 32 (12), 1057–1060, doi: 10.1130/G20896.1.

Algeo, T.J., Maynard, J.B., 2004: Trace-element behavior and redox facies in core shales of Upper Pennsylvnian Kansas-type cyclothems. Chemical Geology 206, 289–318, doi: 10.1016/j.chemgeo.2003.12.009.

Algeo, T.J., Lyons, T.W., 2006: Mo-total organic carbon covariation in modern anoxic marine environments: Implications for analysis of paleoredox and paleohydrographic conditions. Paleoceanography 21, PA1016, doi: 10.1029/2004PA001112.

Algeo, T.J., Maynard, J.B., 2008: Trace-metal covariation as a guide to water-mass conditions in ancient anoxic marine environments. Geosphere 4 (5), 872–887, doi: 10.1130/GES00174.1.

Algeo, T.J., Rowe, H., 2012: Paleoceanographic applications of trace-metal concentration data. Chemical Geology 324-325, 6–18, doi:10.1016/j.chemgeo.2011.09.002.

Aquit, M., Kuhnt, W., Holbourn, A., Chellai, E.H., Lees, J.A., Kluth, O., Jabour, H., 2017. Complete archive of late Turonian to early Campanian sedimentary deposition in newly drilled cores from the Tarfaya Basin, SW Morocco. Geological Society of America Bulletin 129, 137–151.

Bailey, T.R., Rosenthal, Y., McArthur, J.M., van de Schootbrugge, B., Thirlwall, M.F., 2003. Paleoceanographic changes of the Late Pliensbachian–Early Toarcian interval: a possible link to the genesis of an Oceanic Anoxic Event. Earth and Planetary Science Letters 212, 307–320.

Berner, R.A., Raiswell, R., 1983: Burial of organic carbon and pyrite sulfur in sediments over Phanerozoic time: a new theory. Geochimica et Cosmochimica Acta 47, 855–862.

Berner, E.K., Berner, R.A., 1996: Global Environment: Water, Air and Geochemical Cycles. Prentice Hall, Upper Saddle River, N.J., 488 p.

Berner, Z.A., Puchelt, H., Nöltner, T., Kramar, U., 2013: Pyrite geochemistry in the Toarcian Posidonia Shale of south-west Germany: Evidence for contrasting trace-element patterns of diagenetic and syngenetic pyrites. Sedimentology 60, 548-573, doi: 10.1111/j.1365-3091.2012.01350.x.

Bodin, S., Krencker, F.-N., Kothe, T., Hoffmann, R., Mattioli, E., Heimhofer, U., Kabiri, L., 2016: Perturbation of the carbon cycle during the late Pliensbachian – early Toarcian: New insight from high-resolution carbon isotope records in Morocco. Journal of African Earth Sciences 116, 89–104, doi: 10.1016/j.jafrearsci.2015.12.018.

Boström, K., Valdes, S., 1969: Arsenic in ocean floors. Lithos 2, 351–360.

Boström, K., Peterson, M.N.A., 1969: The origin of aluminium-poor ferromanganoan sediments in areas of high heat flow on the East Pacific Rise. Marine Geology 7, 427–447.

Boulila, S., Hinnov, L.A., 2015: Comment on "Chronology of the Early Toarcian environmental crisis in the Lorraine Sub-Basin (NE Paris Basin)" by W. Ruebsam, P. Münzberger, and L. Schwark [Earth and Planetary Science Letters 404 (2014) 273–282]. Earth Planet. Sci Lett. 416, 143–146.

Boulila, S., Hinnov, L.A., 2017: A review of tempo and scale of the early Jurassic Toarcian OAE: implications for carbon cycle and sea level variations. Newsletters on Stratigraphy, doi: 10.1127/nos/2017/0374.

Boulila, S., Galbrun, B., Huret, E., Hinnov, L.A., Rouget, I., Gardin, S., Bartolini, A., 2014: Astronomical calibration of the Toarcian Stage: implications for sequence stratigraphy and duration of the early Toarcian OAE. Earth Planet. Sci Lett. 386, 98–111.

Boyle, E.D, 1983: Manganese carbonate overgrowths on foraminifera test. Geochimica et Cosmochimica Acta 47, 1815–1819.

Calvert, S.E., 1976: The mineralogy and geochemistry of near-shore sediments. In: Riley, J.P. and Chester, R. (Eds.), Chemical Oceanography, v. 6, Academic Press, London, p. 187–280.

Caruthers, A.H., Smith, P.L., Gröcke, D.R., 2013: The Pliensbachian-Toarcian (Early Jurassic) extinction, a global multi-phased event. Palaeogeography, Palaeoclimatology, Palaeoecology 386, 104-118, doi: 10.1016/j.palaeo.2013.05.010

Caswell, B.A., Coe A.L., Cohen, A.S., 2009: New range data for marine invertebrate species across the early Toarcian (Early Jurassic) mass extinction. J. Geol. Soc. Lond. 166, 859–872.

Chen, J., Chen, Y., Liu, L., Ji, J., Balsam, W., Sun, Y., Lu, H., 2006: Zr/Rb ratio in the Chinese loess sequences and its implication for changes in the East Asian winter monsoon strength. Geochimica et Cosmochimica Acta 70, 1471–1482, doi: 10.1016/j.gca.2005.11.029.

Cohen, A.S., Coe, A.L., Harding, S.M., Schwark, L., 2004: Osmium isotope evidence for the regulation of atmospheric CO_2 by continental weathering. Geology 32 (2), 157–160, doi: 10.1130/G20158.1.

Cope, J.C.W., Getty, T.A., Howarth, M.K., Morton, N., Torrens, H.S., 1980: A correlation of Jurassic rocks in the British Isles. Part One: Introduction and Lower Jurassic. Geological Society of London Special Report 14, 1–73.

Dahl, T.W., Ruhl, M., Hammarlund, E.U., Canfield, D.E., Rosing, M.T., Bjerrum, C.J., 2013: Tracing euxinia by molybdenum concentrations in sediments using handheld X-ray fluorescence spectroscopy (HHXRF). Chemical Geology, 360–361, 241–251.

Danise, S., Twitchett, R.J., Little, C.T.S., Clémence, M.-E., 2013: The impact of global warming and anoxia on marine benthic community dynamics: an example from the Toarcian (Early Jurassi). PloS ONE 8 (2), e56255, doi: 10.1371/journal.pone.0056255.

Danise, S., Twitchett, R.J., Little, C.T.S., 2015: Environmental controls on Jurassic marine ecosystems during global warming. Geology 43 (3), 263–266, doi: 10.1130/G36390.1.

Dickson, A.J., Jenkyns, H.C., Porcelli, D., van den Boorn, S., Idiz, E., 2016. Basin-scale controls on the molybdenum-isotope composition of seawater during Oceanic Anoxic Event 2 (Late Cretaceous). Geochimica et Cosmochimica Acta 178, 291–306.

Dickson, A.J., Gill, B.C., Ruhl, M., Jenkyns, H.C., Porcelli, D., Idiz, E., Lyons, T.W., van den Boorn, S., 2017. Molybdenum-isotope chemostratigraphy and paleoceanography of the Toarcian Oceanic Anoxic Event (Early Jurassic). Paleoceanography 32, 813–829, doi: 10.1002/2016PA003048.

Elderfield, H., 1976. Hydrogenous material in marine sediments: excluding manganese nodules. In: Riley, J.P. and Chester, R. (Eds.), Chemical Oceanography, v. 5, Academic Press, London, p. 191.

Faure, G. 1998. Principles and Applications of Geochemistry, Simon and Schuster, New York.

Gale, A.S., Hardenbol, J., Hathway, B., Kennedy, W.J., Young, J.R., Phansalkar, V., 2002. Global correlation of Cenomanian (Upper Cretaceous) sequences: Evidence for Milankovitch control on sea level. Geology 30, 291–294, doi:10.1130/0091-7613(2002)030<0291:GCOCUC>2.0.CO;2

Gély, J.P., Lorenz, J., 2006: Lias and Dogger series of the Paris Basin (France): syn-sedimentary tectonic and palaeogeographic reconstructions for each ammonite biozonation level. Geobios, 39 (5), 631–649.

Gill, B.C., Lyons, T.W., Jenkyns, H.C., 2011: A global perturbation to the sulfur cycle during the Toarcian oceanic Anoxic Event. Earth and Planetary Science Letters 312, 484–496, doi: 10.1016/j.epsl.2011.10.030.

Goldberg, T., Poulton, S.W., Wagner, T., Kolonic, S.F., Rehkämper, M., 2016. Molybdenum drawdown during Cretaceous Oceanic Anoxic Event 2. Earth and Planetary Science Letters 440, 81–91.

Govin, A., Holzwarth, U., Heslop, D., Ford Keeling, L., Zabel, M., Mulitza, S., Collins, J.A, Chiessi, C.M., 2012. Distribution of major elements in Atlantic surface sediments (36°N-49°S): Imprint of terrigenous input and continental weathering. Geochemistry Geophysics Geosystems 13, 1–23, doi:10.1029/2011GC003785.

Gröcke, D.R., 2002. The carbon isotope composition of ancient CO_2 based on higher-plant organic matter. Philosophical Transactions of the Royal Society Series A 360:633–658. doi:10.1098/rsta.2001.0965

Hallam, A., 2001. A review of the broad pattern of Jurassic sea-level changes and their possible causes in the light of current knowledge. Palaeogeography, Palaeoclimatology, Palaeoecology 167, 23–37.

Hammer, Ø., Harper, D.A.T., Ryan, P.D., 2001. PAST: Paleontological statistics software package for education and data analysis. Paleontologia Electronica 4(1), art. 4, 1–9. http://palaeo-electronica.org/2001_1/past/issue1_01.htm

Harries, P.J., Little, C.T.S., 1999: The early Toarcian (Early Jurassic) and the Cenomanian-Turonian (Late Cretaceous) mass extinctions: similarities and contrasts. Palaeogeography, Palaeoclimatology, Palaeoecology 154, 39–66, doi: 10.1016/S0031-0182(99)00086-3.

Hermoso, M., Le Callonec, L., Minoletti, F., Renard, M., Hesselbo, S.P., 2009: Expression of the Early Toarcian negative carbon-isotope excursion in separated carbonate microfractions (Jurassic, Paris Basin). Earth and Planetary Science Letters 277, 194–203, doi: 10.1016/j.epsl.2008.10.013.

Hermoso, M., Minoletti, F., Rickaby, R.E.M., Hesselbo, S.P., Baudin, F., Jenkyns, H.C., 2012: Dynamics of a stepped carbon-isotope excursion: Ultra high-resolution study of Early Toarcian environmental change. Earth and Planetary Science Letters 319-320, 45–54, doi: 10.1016/j.epsl.2011.12.021.

Hermoso, M., Minoletti, F., Pellenard, R., 2013: Black shale deposition during Toarcian super-greenhouse driven by sea level. Climate of the Past 9, 2703–2712, doi: 10.5194/cp-9-2703-2013.

Hesselbo, S.P., 2008: Sequence stratigraphy and inferred relative sea-level change from the onshore British Jurassic. Proceedings of the Geologists' Association 119, 19–34.

Hesselbo, S.P., Jenkyns, H.C., 1995: A comparison of the Hettangian to Bajocian successions of Dorset and Yorkshire, in Taylor, P.D. (ed.): Field Geology of the British Jurassic. Geological Society, London, pp.105-150.

Hesselbo, S.P., Jenkyns, H.C. 1998. British Lower Jurassic sequence stratigraphy. In (de Graciansky, P.C., Hardenbol, J., Jacquin, T., Farley, M., Vail, P.R.; eds) Mesozoic– Cenozoic Sequence Stratigraphy of European Basins. Society for Sedimentary Geology (SEPM), Special Publication 60, 561–581.

Hesselbo, S.P., Pienkowski, G., 2011: Stepwise atmospheric carbon-isotope excursion during the Toarcian Oceanic Anoxic Event (Early Jurassic, Polish Basin). Earth and Planetary Science Letters 301, 365–372, doi: 1016/j.epsl.2010.11.021

Hesselbo, S.P., Gröcke, D.R., Jenkyns, H.C., Bjerrum, C.J., Farrimond, P., Morgans Bell, H.S., Green, O.R., 2000: Massive dissociation of gas hydrate during a Jurassic oceanic anoxic event. Nature 406, 392–395.

Hesselbo, S.P., Jenkyns, H.C., Duarte, L.V., Oliveira, L.C.V., 2007: Carbon-isotope record of the Early Jurassic (Toarcian) Oceanic Anoxic Event from fossil wood and marine carbonate (Lusitanian Basin, Portugal). Earth and Planetary Science Letters 253, 455–470, doi: 10.1016/j.epsl.2006.11.009.

Hetzel, A., Böttcher, M.E., Wortmann, U.G., Brumsack, H.-J., 2009: Paleo-redox conditions during OAE 2 reflected in Demerara Rise sediment geochemistry (ODP Leg 207). Palaeogeography, Palaeoclimatology, Palaeoecology 273, 302-328, doi: 10.1016/j.palaeo.2008.11.005.

Howarth, M.K., 1955: Domerian of the Yorkshire coast. Proceedings of the Yorkshire Geological Society 30 (2-10), 147–175.

Howarth, M.K., 1962: The Jet Rock Series and the Alum Shale Series of the Yorkshire coast. Proceedings of the Yorkshire Geological Society 33 (4-18), 381–422.

Howarth, M.K., 1973: The stratigraphy and ammonite fauna of the Upper Liasic Grey Shales of the Yorkshire coast. British Museum (Natural History).

Howarth, M.K., 2002: The Lower Lias of Robin Hood's Bay, Yorkshire, and the work of Leslie Bairstow. Bulletin of the Natural History Museum: Geology Series, v. 58, p. 81-152.

Huang, C., Hesselbo, S.P., 2014. Pacing of the Toarcian Oceanic Anoxic Event (Early Jurassic) from astronomical correlation of marine sections. Gondwana Research 25, 1348–1356, doi: 10.1016/j.gr.2013.06.023.

Huang, C., Hesselbo, S.P., Hinnov, L.A., 2010. Astrochronology of the Late Jurassic Kimmeridge Clay (Dorset, England) and implications for Earth system processes. Earth and Planetary Science Letters, 289, 242–255, doi:10.1016/j.epsl.2009.11.013

Husson, D., Thibault, N., Galbrun, B., Gardin, S., Minoletti, F., Sageman, B., Huret, E., 2014: Lower Maastrichtian cyclostratigraphy of the Bidart section (Basque Country, SW France): A remarkable record of precessional forcing. Palaeogeography, Palaeoclimatology, Palaeoecology 395, 176–197, doi: 10.1016/j.paaeo.2013.12.008.

Jenkyns, H.C., 1988: The Early Toarcian (Jurassic) anoxic event – stratigraphic, sedimentary, and geochemical evidence. American Journal of Science 288 (2), 101–151, doi: 10.2475/ajs.288.2.101.

Kemp, D.B., Coe, A.L., Cohen, A.S., Schwark, L., 2005: Astronomical pacing of methane release in the Early Jurassic period. Nature 437, 396–399, doi: 10.1038/nature04037.

Kemp, D.B., Coe, A.L., Cohen, A.S., Weedon, G.P., 2011: Astronomical forcing and chronology of the early Toarcian (Early Jurassic) oceanic anoxic event in Yorkshire, UK. Palaeoceanography 26, PA4210, doi: 10.1029/2011PA002122.

Knox, R.W.O'B., 1984: Lithostratigraphy and depositional history of the late Toarcian sequence at Ravenscar, Yorkshire. Proceedings of the Yorkshire Geological Society 45 (1-2), 99–108.

Large, R.R., Bull, S.W., Maslennikov, V.V., 2011: A Carbonaceous Sedimentary Source-Rock Model for Carlin-type and Orogenic Gold Deposits. Economic Geology 106, 331–358.

Lenniger, M, Nøhr-Hansen, H., Hills, L.V., Bjerrum, C.J., 2014. Arctic black shale formation during Cretaceous Oceanic Anoxic Event 2. Geology, 42, 799–802, doi: 10.1130/G35732.1

Liu, L., Chen, J., Ji, J., Chen, Y., 2004: Comparison of paleoclimatic change from Zr/Rb ratios in Chinese loess with marine isotope records over the 2.6-1.2 Ma BP interval. Geophysical Research Letters 31, L15204, doi: 10.1029/2004GL019693.

Little, C.T.S., Benton, M.J., 1995: Early Jurassic mass extinction: A global long-term event. Geology 23 (6), 495–498.

Littler, K., Hesselbo, S.P., Jenkyns, H.C., 2010: A carbon-isotope perturbation at the Pliensbachian-Toarcian boundary: evidence from the Lias Group, NE England. Geological Magazine 147 (2), 181–192, doi: 10.1017/S0016756809990458.

Maher, W., Butler, E., 1988: Arsenic in the marine environment. Applied Organometallic Chemistry 2, 191–214.

Martin, K.D., 2004: a re-evaluation of the relationship between trace fossils and dysoxia. In: McIlroy. D. (Ed.), The Application of Ichnology to Palaeoenvironmental and Stratigraphic Analysis. Geological Society, Special Publications 228, 141–156.

Martinez, M., Krencker, F.-N., Mattioli, E., Bodin, S., 2017. Orbital chronology of the Pliensbachian – Toarcian transition from the Central High Atlas Basin (Morocco). Newsletters on Stratigraphy 50, 47–69.

Matschullat, J., 2000: Arsenic in the geosphere – a review. The Science of the Total Environment 249, 297–312.

McArthur, J.M., Donovan, D.T., Thirlwall, M.F., Fouke, B.W., Mattey, D., 2000. Strontium isotope profile of the early Toarcian (Jurassic) oceanic anoxic event, the duration of ammonite biozones, and belemnite palaeotemperatures. Earth and Planetary Science Letters 179, 269–285.

McArthur, J.M., Algeo, T.J., van de Schootbrugge, B., Li, Q., Howarth, R.J., 2008: Basinal restriction, black shales, Re-Os dating, and the Early Toarcian (Jurassic) oceanic anoxic event. Paleoceanography 23, PA4217, doi: 10.1029/2008PA001607.

McArthur, J.M., Steuber, T., Page, K.N., Landman, N.H., 2016: Sr-Isotope Stratigraphy: Assigning Time in the Campanian, Pliensbachian, Toarcian, and Valanginian. The Journal of Geology 124, 569–586.

McElwain, J.C., Wade-Murphy, J., Hesselbo, S.P., 2005: Changes in carbon dioxide during an oceanic anoxic event linked to intrusion into Gondwana coals. Nature 435, 479–782.

Meyers, S.R., 2012. Seeing red in cyclic stratigraphy: Spectral noise estimation for astrochronology. Paleoceanography 27, PA3228, doi: 10.1029/2012PA002307.

Meyers, S.R., 2014. Astrochron: An R package for astrochronology, [Available at http://cran.r-project.org/package=astrochron]

Mejía-Piña, K.G., Huerta-Diaz, M.A., Gonzáles-Yajimovich, O., 2016: Calibration of handheld X-ray fluorescence (XRF) equipment for optimum determination of elemental concentrations in sediment samples. Talanta 161, 359–367, doi: 10.1016/j.talanta.2016.08.066.

Montero-Serrano, J.C., Föllmi, K., Adatte, T., Spangenberg, J.E., Tribovillard, N.P., Fantasia, A., Suan, G., 2015. Continental weathering and redox conditions during the early Toarcian Oceanic Anoxic Events in the northwestern Tethys: Insights from the Posidonia Shale section in the Swiss Jura Mountains. Palaeogeography, Palaeoclimatology, Palaeoecology 429, 83–99, doi: 10.1016/j.palaeo.2015.03.043.

Morris, K.A., 1979: A classification of Jurassic marine shale sequences: an example from the Toarcian (Lower Jurassic) of Great Britain. Palaeogeography, Palaeoclimatology, Palaeoecology 26, 117–126.

Müller, T., Price, G.D., Bajnai, D., Nyerges, A., Kesjar, D., Raucsik, B., Varga, A., Judik, K., Fekete, J., May, Z., Pálfy, J., 2017: New multiproxy record of the Jenkyns Event (alsoknown as the Toarcian Oceanic Anoxic Event) from the Mecsek Mountains (Hungary): Differences, duration and drivers. Sedimentology 64, 66–86, doi: 10.1111/sed.12332.

Newton, R.J., Reeves, E.P., Kafousia, N., Wignall, P.B., Bottrell, S.H., Sha, J.-G., 2011: Low marine sulfate concentrations and the isotlation of the European epicontinental sea during the Early Jurassic. Geology 39 (1), 7–10, doi: 10.1130/G31326.1.

Niebuhr, B., 2005: Geochemistry and time-series analysis of orbitally forced Upper Cretaceous marl-limestone rhytmites (Lehrte West Syncline, northern Germany). Geological Magazine 142, 31–55.

O'Brien, N.R., 1990: Significance of lamination in Toarcian (Lower Jurassic) shales from Yorkshire, Great Britain. Sedimentary Geology 67, 25–34.

Ogg, J., Ogg, G., Gradstein, F., 2016. A Concise Geologic Time Scale. Elsevier, 240 p.

Pearce, C.R., Cohen, A.S., Coe, A.L., Burton, K.W., 2008: Molybdenum isotope evidence for global ocean anoxia coupled with perturbations to the carbon cycle during the Early Jurassic. Geology 36 (3), 231–234, doi: 10.1130/G24446A.1.

Peterson, M.L., Carpenter, R., 1986: Arsenic distributions in porewaters and sediments of Puget Sound, Lake Washington, the Washington coast and Saanich Inlet, B.C. Geochimica et Cosmochimica Acta 50, 353–369.

Peti, L., Thibault, N., Clémence, M.-E., Korte, C., Dommergues, J.-L., Bougeault, C., Pellenard, P., Jelby, M.E., Ullmann, C.V., 2017. Sinemurian–Pliensbachian calcareous nannofossil biostratigraphy and organic carbon isotope stratigraphy in the Paris Basin: Calibration to the ammonite biozonation of NW Europe. Palaeogeography, Palaeoclimatology, Palaeoecology 468, 142–161.

Potts, P.J., West, M., 2008. Portable X-ray Fluorescence Spectrometry: Capabilities for In Situ Analysis. RSC publishing, London, UK, 291 pp.

Powell, J.H., 2010: Jurassic sedimentation in the Cleveland Basin: a review. Proceedings of the Yorkshire Geological Society 58 (1), 21–72.

Pye, K., 1987: Aeolian Dust and Dust Deposits. Academic Press, San Diego, 334 p.

Pye, K., Prinsley, D.H., 1986: Microfabric, mineralogy and early diagenetic history of the Whitby Mudstone Formation (Toarcian), Cleveland Basin, U.K. Geological Magazine 123, 191–203.

Raiswell, R., Berner, R.A., 1985: Pyrite formation in euxinic and semi-euxinic sediments. American Journal of Science 285, 710–724.

Raiswell, R., Buckley, F., Berner, R.A., Anderson, T.F., 1988: Degree of pyritization of iron a a paleoenvironmental indicator of bottom-water oxygenation. Journal of Sedimentary Research 58 (5), 812–819.

Ruebsam, W., Münzberger, P., Schwark, L., 2014: Chronology of the Early Toarcian environmental crisis in the Lorraine Sub-Basin (NE Paris Basin). Earth Planet. Sci. Lett. 404, 273–282.

Ruebsam, W., Münzberger, P., Schwark, L., 2015: Reply to the comment by Boulila and Hinnov towards "Chronology of the Early Toarcian environmental crisis in the Lorraine Sub-Basin (NE Paris Basin)" by W. Ruebsam, P. Münzberger, and L. Schwark [Earth and Planetary Science Letters 404 (2014) 273–282]. Earth Planet. Sci. Lett. 416, 147–150.

Saltzman, M.R., Thomas, E., 2012. Carbon Isotope Stratigraphy. In: Gradstein, F..et al. (Eds.) The Geologic Time Scale 2012. Elsevier, pp. 207–232.

Sames, B., Wagreich, M., Wendler, J. E., Haq, B. U., Conrad, C. P., Melinte-Dobrinescu, M. C., Hu, X., Wendler, I., Wolfgring, E., Yilmaz, I. Ö., and Zorina, S. O., 2016, Review: Short-term sea-level changes in a greenhouse world - A view from the Cretaceous: Palaeogeography, Palaeoclimatology, Palaeoecology 441, 393–411.

Sforna, M.C., Philipot, P., Somogyi, A., van Zuilen, M.A., Medjoubi, K., Schoepp-Cothenet, B., Nitschke, W., Visscher, P.T., 2014: Evidence for arsenic metabolism and cycling by microorganisms 2.7 billion years ago. Nature Geoscience 7, 811–815.

Suan, G., B. Pittet, I. Bour, E. Mattioli, L. V. Duarte, and S. Mailliot, 2008: Duration of the Early Toarcian carbon isotope excursion deduced from spectral analysis: Consequence for its possible causes. Earth Planet. Sci. Lett., 267, 666–679.

Suan, G., Mattioli, E., Pittet, B., Lécuyer, C., Suchéras-Marx, B., Duarte, L.V., Philippe, M., Reggiani, L., Martineau, F., 2010: Secular environmental precursors to Early Toarcian (Jurassic) extreme climate changes. Earth and Planetary Science Letters 290, 448–458, doi: 10.1016/j.epsl.2009.12.047.

Taner, M.T., 2000. Attributes Revisited. Technical Publication, Rock Solid Images, Inc., Houston, Texas (http://www.rocksolidimages.com/pdf/attrib_revisited.htm).

Tribovillard, N., Algeo, T.J., Lyons, T., Riboulleau, A., 2006: Trace metals as paleoredox and paleoproductivity proxies: An update. Chemical Geology 232, 12–32, doi: 10.1016/j.chemgeo.2006.02.012.

Turekian, K.K., Wedepohl, K.H., 1961: Distribution of the elements in some major units of the Earth's crust. Geological Society of America Bulletin 72, 175–192.

Ullmann, C.V., Thibault, N., Ruhl, M., Hesselbo, S.P., Korte, C., 2014: Effect of a Jurassic Oceanic Anoxic Event on belemnite ecology and evolution. PNAS 111, 10073–10076, doi: 10.1073/pnas.1320156111

Vortisch, W., McMinn, J., Lindström, M., Starke, K., 1981. Arsenic enrichment at the Cambro-Ordovician boundary in south Sweden. GFF 104, 211–218.

Waltham, D., 2015: Milankovitch period uncertainties and their impact on cyclostratigraphy. Journal of Sedimentary Research 85, 990–998.

Weaver, C.E., 1967: Potassium, illite and the ocean. Geochimica et Cosmochimica Acta 31, 2181–2196.

Weaver, C.E., 1989: Clays, muds, and shales (Vol. 44). Elsevier.

Wedepohl, K.H., 1971: Environmental influences on the chemical composition of shales and clays. Physics and Chemistry of the Earth 8, 307–333.

Wignall, P.B., Newton, R.J., Little, C.T.S., 2005: The timing of paleoenvironmental change and cause-and-effect relationships during the early Jurassic mass extinction in Europe. American Journal of Science 305, 1014–1032, doi: 10.2475/ajs.305.10.1014.

Additional available online or on demand (nt@ign.ku.dk)

Appendix A: Results of the hand-held XRF measurements in ppm presented along with the stratigraphy of the different sections.

Appendix B: Assessment of the quality of As data via HH-XRF measurements.

Appendix C: New $\delta^{13}C_{org}$ data analysed for this study in the Mulgrave shale Mb. of Saltwick Nab.

Appendix D: data matrix used for the multivariate statistics (original values have been centred and reduced by the mean and standard deviation of each variable)